Nitric oxide is a volume transmitter regulating postsynaptic excitability at a glutamatergic synapse

Joern R. Steinert[1], Cornelia Kopp-Scheinpflug[2], Claire Baker[1], R.A. John Challiss[3], Raj Mistry[3], Martin D. Haustein[1], Sarah J. Griffin[1], Huaxia Tong[1], Bruce P. Graham[4], Ian D. Forsythe[1].

1. MRC Toxicology Unit, Hodgkin Building, University of Leicester, LE1 9HN. UK
2. Institute of Biology II, Faculty of Biosciences, Pharmacy and Psychology, University of Leipzig, Talstraße 33, 04103 Leipzig. Germany.
3. Department of Cell Physiology & Pharmacology, University of Leicester, LE1 9HN. UK.
4. Department of Computing Science and Mathematics, University of Stirling. FK9 4LA. UK.

Running title: NO mediates volume modulation of neuronal excitability

Corresponding Author: Professor Ian D. Forsythe, MRC Toxicology Unit, University of Leicester, Leicester LE1 9HN. UK. email: idf@le.ac.uk

Acknowledgments: Many thanks to Volko Straub for comments on a draft manuscript. We are grateful to Paul L. Huang for the generous provision of the KN2 transgenic mice. This work was supported by the following organisations: Medical Research Council, Deutsche Forschungsgemeinschaft (Ru 390/18-1), Biotechnology and Biological Sciences Research Council, and Deafness Research UK.

Summary

Neuronal nitric oxide synthase (nNOS) is broadly expressed in the brain and associated with synaptic plasticity through NMDAR -mediated calcium influx. However, its physiological activation and the mechanisms by which nitric oxide (NO) influences synaptic transmission have proved elusive. Here, we exploit the unique input-specificity of the calyx of Held to characterize NO modulation at this glutamatergic synapse in the auditory pathway. NO is generated in an activity-dependent manner by principle neurons receiving a calyceal synaptic input. It acts in the target and adjacent inactive neurons to modulate excitability and synaptic efficacy, inhibiting postsynaptic Kv3 potassium currents (via phosphorylation), reducing EPSCs and so increasing action potential duration and reducing the fidelity of transmission. We conclude that NO serves as a volume transmitter and slow dynamic modulator, integrating spontaneous and evoked neuronal firing, providing an index of global activity and regulating information transmission across a population of active and inactive neurons.

Introduction

Nitric oxide is a crucial signaling molecule in cardiovascular (Ignarro et al., 1987; Palmer et al., 1987), reproductive (Hurt et al., 2006), immune (Bogdan, 2001) and central nervous systems (Bon and Garthwaite, 2003; Bredt et al., 1990). NO exhibits properties ideally suited for a trans-cellular messenger; being highly soluble and mobile (unimpeded by cell membranes), widely synthesized and of limited life-time. It acts via a well characterized NO-cGMP pathway (Southam and Garthwaite, 1993), although S-nitrosylation of proteins, generation of reactive oxygen species and regulation of cellular respiration also contribute to physiological and pathological roles (Ahern et al., 2002). In the brain, nNOS is expressed widely in the neocortex, cerebellum and hippocampus and is closely associated with NMDAR (Brenman et al., 1996) and synaptic plasticity (Garthwaite, 2008; Hopper and Garthwaite, 2006; Jacoby et al., 2001; Son et al., 1996). NO has the potential to act as an anterograde or retrograde modulator, but its mechanisms of controlling neuronal excitability in the brain are not well characterized.

We have exploited a glutamatergic synapse in the auditory brainstem, called the calyx of Held (Forsythe, 1994; Schneggenburger and Forsythe, 2006; von Gersdorff and Borst, 2002) to study the cellular mechanism of NO signaling. This giant synapse forms on principal neurons in the medial nucleus of the trapezoid body (MNTB). Each neuron receives one calyx which generates a stereotypical dual component response: a fast AMPAR-mediated and slow

NMDAR-mediated EPSC (Barnes-Davies and Forsythe, 1995; Forsythe and Westbrook, 1988; Futai et al., 2001; Joshi and Wang, 2002). The morphology of the calyx is analogous to an axon terminal field enveloping a single neuronal soma, so providing the ultimate input-specificity of one synapse to one target neuron. This giant synapse serves as a relay in pathways responsible for sound localization, by comparison of auditory information from both cochleae (Oertel, 1999). The MNTB expresses high levels of several crucial elements in NO signaling, including nNOS and soluble guanylyl cyclase (sGC) (Fessenden et al., 1999; Lein et al., 2007).

Concepts of plasticity often focus on changes in synaptic strength, but the synaptic response must also integrate with the intrinsic voltage-gated currents of the target neuron to generate an action potential (AP) output. Therefore modulation of these postsynaptic intrinsic conductances contributes to neuronal excitability (Daoudal and Debanne, 2003; Marder and Prinz, 2002) and also synaptic efficacy. For example in the MNTB, AP firing threshold and excitability are regulated by Kv1 channels (Brew and Forsythe, 2005; Dodson et al., 2002) while AP duration and firing rates are influenced by Kv3 channels (Wang et al., 1998). Kv3 channels are widely expressed in fast-spiking neurons (Rudy and McBain, 2001) and in the auditory system their activity is regulated by sound-evoked changes in phosphorylation (Song et al., 2005). In this paper we identify a new form of activity-dependent signaling mediated by NO, which acts over relatively slow timescales (5-30min) consistent with a physiological role in tuning a neuronal population to the volume-average of local spontaneous and evoked synaptic activity.

Results

nNOS is expressed at postsynaptic sites in MNTB neurons

MNTB neurons and the calyx of Held express the voltage-gated K^+ channel Kv3.1b (Elezgarai et al., 2003; Wang et al., 1998) and antibodies to this channel clearly show the bilateral location of the MNTB in transverse cryostat sections of the superior olivary complex (SOC, Figure 1A) in the auditory brainstem. In this region endothelial NOS (eNOS) was localized to blood vessels on the ventral surface and within capillaries, but was not detectable in MNTB neurons or glial cells, as emphasized by the separate localization of eNOS and Kv3.1b. In contrast, an antibody to nNOS showed strong labeling of the MNTB (Figure 1Aiv). Co-labeling of Kv3.1b with the vesicular glutamate transporter-2 (vGLUT2) (Billups, 2005) and with nNOS showed Kv3.1b (green, Figure 1B) was largely present in membranes, while nNOS (red) was located in the cytoplasm of MNTB principal neurons. The localization of either vGLUT2 (green, Figure 1C) or PSD-95 (green, Figure 1D) with Kv3.1b clearly shows

the synaptic profiles of the calyx around each neuron, emphasizing the postsynaptic cytoplasmic location of nNOS (red). DAPI staining showed principal neuron nuclei with prominent nucleoli (Figure 1C, D, *).

Nitric oxide is generated on synaptic stimulation

To investigate the role of NO in auditory brainstem signaling we used the fluorescent probe, DAR-4M (Kojima et al., 2001) to monitor NO production in brainstem slice preparations of the mouse SOC. Presynaptic calyceal APs were evoked using midline bipolar stimulation at 36-37^{o}C (Billups et al., 2002) and stimulation rates of up to 100Hz. These rates of synaptic stimulation were well within the auditory pathway physiological range for both spontaneous and sound-driven inputs. High levels of spontaneous firing are a feature of the auditory pathway (Liberman and Oliver, 1984) with the mouse MNTB having spontaneous rates between 0-150Hz and peak sound-evoked firing rates can exceed 700Hz *in vivo* (Kopp-Scheinpflug et al., 2003a). The slice preparation divides MNTB neurons into two groups: those with an intact calyceal input (connected) and the majority, without an intact calyx (non-connected) caused by severing the axon when cutting the brain slice. Spontaneous AP firing of MNTB neurons in an *in vitro* slice is rare (<<1Hz) since there is no intact input from the cochlea.

Following a 5min control period (Figure 2A), calyceal axons were stimulated (indicated by each arrow) at 100Hz, 7 times (each 120s) and DAR-4M fluorescence changes were monitored. A connected MNTB neuron possessing an intact calyceal input ('connected') showed a slow increase in DAR-4M fluorescence (Figure 2A, filled symbols, data expressed as $\Delta F/F_0$ [$t_{1/2}$=679±42s, n=14]). The non-connected cell showed a smaller magnitude change (open symbols) but no change in fluorescence was observed in another preparation in the absence of stimulation (grey symbols). The DAR-4M/NO reaction is irreversible, so termination of NO production is observed as a declining rate of increase following stimulation; the asymptote is not dye depletion since application of the NO-donor sodium nitroprusside (SNP) increased fluorescence of both connected and non-connected neurons to a similar level. In averaged data from 3 connected neurons (Figure 2B) delivery of two identical 100Hz trains led to a biphasic rise of DAR-4M fluorescence which also increased further with SNP.

To aid quantification and pharmacological characterization of NO production we used two identical consecutive stimulus trains (Figure 2C). Each is referred to as a 'Synaptic Stimulus Protocol' (SSP); consisting of a 60s, 100Hz train with a 50% duty cycle (SSP = 60s @100Hz, 500ms on, 500ms off; i.e. an average of 50Hz over 1min). The two SSPs were separated by

1000s and each caused increases in $[Ca^{2+}]_i$ in connected MNTB neurons and a reproducible DAR-4M fluorescence change (in paired experiments on the same slice). A single Fura-2 image at 380nm shows (Figure 2C, left) a connected (red circle) and a non-connected (black circle) MNTB neuron with the 340/380nm fluorescence ratio plotted during synaptic stimulation (red and black insets, respectively). The change in DAR-4M fluorescence (ΔF_1) is shown in the middle image and plotted over time in Figure 2C, right ($\Delta F/F_0$). The actions of pharmacological agents were assessed as the ratio of signal differences ($\Delta F_2/\Delta F_1$) between the first control SSP ($\Delta F_1=\Delta F_{1100s}-\Delta F_{100s}$) and the second test SSP ($\Delta F_2=\Delta F_{2000s}-\Delta F_{1000s}$). Figure 2D shows a single cell receiving two SSP stimuli (open symbols) overlaid with data from another slice showing suppression of the SSP2 response by glutamate receptor antagonists (Figure 2D, filled symbols). Because of the continued increase in DAR-4M fluorescence following SSP1, the measured SSP2 fluorescence signal was larger than that for SSP1. The continued accumulation from SSP1 was measured at both ΔF_1 and ΔF_2 time-points (Figure 2E, 1xSSP = Zero, $\Delta F_2/\Delta F_1= 0.35\pm0.28$, n=3). Because of this small continued increase, the dashed line in the summary data (Figure 2E) gives the best estimate for a zero response to SSP2. Under control conditions, $\Delta F_2/\Delta F_1$ is larger than 1 ($\Delta F_2/\Delta F_1=1.51\pm0.12$, n=13), suggesting potentiation of NO production for the second stimulus. Perfusion of glutamate receptor antagonists following SSP1, resulted in reduced $\Delta F_2/\Delta F_1$ ratios for NO production (Figure 2E, filled bars) and reduced $[Ca^{2+}]_i$ for SSP2 (open bars). The NMDAR antagonist AP-5 blocked NO accumulation at all animal ages tested (up to P21, Figure S4B). The AMPAR antagonist DNQX also partially blocks NMDAR, and so reduced NO accumulation when applied alone, but the absence of NO accumulation in AP-5 implies that Ca^{2+}-permeable AMPAR expressed in the MNTB (Joshi et al., 2004) make little or no contribution to nNOS activation. Competitive NOS antagonists, N-PLA (10μM), L-NMMA (500μM) and 1400W (10μM) each suppressed DAR-4M fluorescence ratios $\Delta F_2/\Delta F_1$ but left SSP2-evoked $[Ca^{2+}]_i$ increases unaffected (Figure 2E, open bars for N-PLA and L-NMMA). These results are consistent with NMDAR and calcium-dependent induction of nNOS and suggest little involvement of endothelial or inducible NOS isoforms (Hopper and Garthwaite, 2006).

Synaptic activity induces cGMP accumulation

A key action of NO is activation of sGC and generation of intracellular cGMP. Measurement of cGMP was performed (using the same *in vitro* slice preparation) in response to perfusion of NO-donors and after presynaptic stimulation (SSP). Low basal cGMP concentrations were enhanced by inhibition of phosphodiesterases (IBMX, 0.5mM) in control non-stimulated

slices (Figure 2F) and were unchanged by perfusion with Bay 41-2272, an allosteric enhancer of the sGC activity (1μM, data not shown) suggesting little basal sGC activity at rest *in vitro*. Perfusion of the NO donor SNAP (100μM) increased cGMP concentrations by two orders of magnitude. Electrical stimulation of the presynaptic axons in the MNTB showed that a physiological stimulus also raised cGMP and this was further potentiated by IBMX. Despite the small number of intact calyceal axons, we still detected strong cGMP production and this increase was blocked by tetrodotoxin or by inhibition of nNOS with N-PLA (10μM) confirming generation of cGMP on synaptic stimulation through a nNOS-dependent mechanism.

Non-synaptic volume-transmission by NO

NO has long been considered a putative volume transmitter, but it is difficult to prove this concept in most brain areas, where synaptic inputs are distributed between many neurons. Visualization of trans-neuronal NO diffusion in the MNTB was achieved using DAR-4M and calcium imaging. Figure 3A shows 2 neurons in which one receives a calyceal input (*, red circle). On delivery of two SSP, this neuron exhibited sustained large changes in $[Ca^{2+}]_i$ (red trace, inset) while a non-innervated neuron (black circle) showed no change in $[Ca^{2+}]_i$ (black trace, inset). Following SSP1, the ΔF_1 image shows a global increase in fluorescence (Figure 3A, ΔF_1) and a plot of the DAR-4M $\Delta F/F_0$ against time (Figure 3A, right) shows clear NO accumulation after SSP1 in both neurons (red, connected; black, non-connected). Perfusion of the NO scavenger, PTIO (Figure 3A, ΔF_2) prior to the second SSP suppressed the fluorescent *increase* in the non-innervated neuron and surrounding tissue (Figure 3A, right, black symbols after SSP2) although the innervated neuron continued to respond (Figure 3A, right, red symbols after SSP2). A line scan for this same data is shown in Figure 3B (data plot along the 100μm white line in Figure 3A). The innervated neuron (*) shows high fluorescence following SSP1 while the non-connected neuron (#) also shows substantial fluorescence (ΔF_1, black trace). Following perfusion by PTIO (ΔF_2, grey trace) the increase in background fluorescence is suppressed everywhere, while the innervated neuron still shows a rise in NO-fluorescence. Averaging the fluorescence intensities for ΔF_1 and ΔF_2 measured over four innervated neurons ("On Cell") versus the 20μm either side of the same neuron ("Off Cell") in the absence (filled bars) and presence of PTIO during the second SSP (grey bars) shows that NO diffusion was prevented by scavenging (Figure 3C).

Further evidence for the diffusion of NO was obtained by estimating NO accumulation with distance from known sources. The NO concentration gradient was estimated from the rate of change of DAR-4M fluorescence and plotted against distance from a single neuron source following one SSP. The rate of change decreased proportionally to the distance from the source neuron (Figure 3D) compared with the response to perfusing an NO-donor, where the gradient did not change with distance. Numerical simulation of NO spread was made within a block of neural tissue (Figure S1). A 20μm diameter spherical constant-rate source of NO gives a highly localized [NO] diffusion curve when subject to inactivation, i.e. NO is scavenged or degraded (Figure 3E, left curve), however, a good fit with the experimental data (Figure 3E, right curve) required potentiation of NO synthesis, which is consistent with the facilitation observed in the paired SSP protocols (Figure 2E). Using physiological levels of spontaneous AP firing, the model predicted basal NO-generation and enhanced synthesis with sound driven activity (Figure S1A, B), so when the tonotopic distribution of spontaneous activity (Smith et al., 1998) is taken into consideration, the model predicts an *in vivo* gradient of NO across the tonotopic axis of the MNTB (Figure S1A, B) which would interact with tonotopic gradients of ionic conductances measured from 'silent' *in vitro* brain slices (discussion).

Further confirmation of the volume transmission hypothesis was obtained by loading single neurons with DAR-4M-AM using a loose patch configuration, thus reducing the background fluorescence from the bulk tissue. In one field of view both labeled cells had intact calyceal inputs (Figure 3F) as indicated by raised intracellular calcium on stimulation (340/380nm ratio traces, red insets). The line-scan across one neuron showed increased fluorescence following synaptic stimulation (F_1) compared to control (F_0). DAR-4M fluorescence is plotted along the line scan for F_0 and F_1 in Figure 3F (right graph). In another experiment two connected neurons flanked one non-connected MNTB neuron (Figure 3G). Line-scans across the non-connected neuron showed SSP-evoked rises in DAR-4M fluorescence, as indicated in the example images F_0 (before) and F_1 (after SSP). Similar data were obtained from 4 such neuron pairs and confirm accumulation of NO in connected as well as in non-connected neurons following synaptic stimulation.

Nitric oxide signaling suppresses postsynaptic Kv3 potassium currents

Whole-cell patch clamp recordings from MNTB neurons with an identified calyceal input, or from other neurons without a functional input showed that both connected (Figure 4A, B, insets show representative traces) and non-connected neurons (Figure 4D, E) had large

voltage-activated outward K^+ currents which were suppressed in both cases on synaptic stimulation. The slow 10-15min time-course of the depression (Figure 4B, E) was mimicked by perfusion of DEA-NONOate (Figure 4C, open triangles in the absence of stimulation, 100μM) and contrasts with the minor run-down observed over 20 minutes recording in slices receiving neither stimulation nor NO-donor (Figure 4C, filled squares). Identical results were obtained with SNP (100μM, n=6, not shown) so individual data for SNP and DEA were combined in later figures. Summary data are plotted as mean absolute current magnitude (measured at +50mV) in Figure 4F, showing the suppression of outward K^+ currents on synaptic stimulation (SSP) by approximately 50% in connected neurons, which was blocked by perfusion of 1400W (10μM, n = 4) during the SSP. Similarly, outward potassium currents were suppressed in non-connected neurons by a SSP and on perfusion of DEA (100μM). Application of SNP (100μM) also reduced high voltage-activated currents (evoked by depolarizations positive to -10mV, Figure 4G), and this suppression was blocked by the sGC inhibitor 1H-(1,2,4)oxadiazolo[4,3-a]quinozalin-1-one (ODQ, 1μM) and occluded by perfusion of low concentrations of tetraethylammonium (TEA, 3mM). This concentration of TEA is selective for Kv3 currents in MNTB neurons (Brew and Forsythe, 2005; Macica et al., 2003) (Figure 4H; summarized in Figure 4I). We conclude that NO is generated in response to stimulation of glutamatergic receptors at the calyx of Held and acts to suppress postsynaptic Kv3 currents within the cell of origin and across a population of active and inactive neurons through a process of volume transmission.

Phosphorylation is a major control mechanism of Kv3 potassium channels (Song et al., 2005); high levels of phosphorylation suppress channel opening, while dephosphorylation increases open probability. Perfusion of the PKG antagonist KT 5823 (1μM) enhanced resting Kv3 currents and blocked the suppression by SNP. The high voltage-activated current was confirmed as Kv3 as it was blocked by perfusion with TEA (3mM) (Figure 4J). In other experiments the phosphatase inhibitor okadaic acid (100nM, included in the patch pipette or bath perfused) rapidly suppressed the high voltage-activated currents (Figure 4K) and occluded the response to NO donors (not shown). The averaged data is plotted in Figure 4L and suggests that native Kv3 channel activity is highly dependent on the equilibrium between phosphorylation and dephosphorylation. The extent to which this mechanism reflects direct versus indirect actions is presently unclear because of the range of kinase signaling converging at the Kv3.1 channel and needs further investigation.

NO inhibits postsynaptic glutamate receptors, but does not change transmitter release

Volume diffusion of NO between neurons and their synaptic terminals means that the net physiological effect of NO modulation could involve both presynaptic and/or postsynaptic effects. Given the broad spectrum of potential NO actions, we next sought to establish which sites of action were of most relevance for modulation of transmission strength by monitoring the effect of NO-donors on MNTB field potentials and by comparing spontaneous and evoked EPSCs at the calyx of Held/MNTB synapse. Perfusion of SNP inhibited the postsynaptic component of the evoked extracellular compound field potentials (Figure S2; C2, postsynaptic) recorded in MNTB following stimulation of the trapezoid body in the brain slice preparation, but it had little or no effect on the presynaptic field potentials (Figure S2; C1, presynaptic) consistent with a postsynaptic mechanism involving reduced synaptic strength, raised firing threshold and/or reduced excitability.

Kv3 channels are present on both presynaptic and postsynaptic membranes. Suppression of presynaptic Kv3 could potentiate transmitter release, due to increased AP duration and calcium influx (Wang and Kaczmarek, 1998), while suppression of postsynaptic Kv3 would modify postsynaptic MNTB excitability and AP waveform, as shown here. Additionally, NO signaling may exert direct actions on transmitter release or modulate postsynaptic glutamate receptors themselves. Patch clamp recordings from innervated MNTB neurons exhibited calyceal EPSCs with a mean amplitude of 7.9nA at the holding potential of -60mV. NO-donors (SNP, 100μM or DEA, 100μM) suppressed the evoked AMPAR-mediated EPSCs by 35±4% (n=7) and slowed the decay kinetics from 0.37±0.07ms to 0.86±0.2ms (HP=-60mV, 37^{o}C, Figure 5A-D). Similar observations were made for NMDAR-mediated currents with a mean amplitudes of 1.8nA (HP=+50mV, Figure 5B-D). The inhibition of both the AMPAR and NMDAR-mediated EPSCs was mimicked by a SSP, and this was blocked by perfusion with the nNOS antagonist 1400W (10μM). Although some of these changes could be mediated by either presynaptic or postsynaptic mechanisms, examination of spontaneous miniature EPSCs (mEPSC) in MNTB neurons clearly shows a postsynaptic mechanism. NO-donors had no significant effect on release probability, since mEPSC frequencies were unchanged on perfusion of SNP ($f_{control}$ = 7.0±2.9Hz; f_{NO} = 6.6±3.8Hz, n=5). But mEPSC amplitudes were reduced by 27.2±2.3% and their decay kinetics slowed to a similar extent as for evoked EPSCs ($mEPSC_{Control}$ = -73.7±4.8pA; $mEPSC_{NO}$ = -53.7±4.2pA; $\tau_{Control}$ = 0.34±0.02ms; τ_{NO} = 0.51±0.01ms; HP= -60mV, $p<0.05$, paired Student's t-test, n=5; Figure 5E, F). Data from the same neuron showed identical changes for evoked EPSCs and mEPSCs

on SNP application (Inset, Figure 5E). Mean data shows comparable significant changes (inset, Figure 5F) and in a further three cases synaptic stimulation with a SSP caused a similar 34.9±11.3% reduction in mEPSC amplitudes. The equivalent depression of amplitude and slowed time-course for both miniature and evoked EPSCs is incompatible with a presynaptic mechanism but is consistent with a postsynaptic modulation of AMPAR and NMDAR and is similar to that reported for AMPAR in the hippocampus (Lei et al., 2000). These results confirm that NO has multiple postsynaptic sites of modulatory action: it suppresses postsynaptic Kv3 potassium channels and reduces and slows the evoked calyceal EPSC.

NO signaling slows the MNTB neuron action potential

Kv3 channels contribute to AP repolarization in MNTB neurons, so the physiological consequence of their inhibition by endogenous NO should be increased AP half-width. Using current clamp recording in the whole-cell patch configuration, APs evoked by current injection had half-widths of 0.40±0.01ms (n=38), as shown in Figure 6A and 6B. Following 10min perfusion of SNP or DEA (each 100μM), AP half-width increased to 0.86±0.07ms (n=15). Similarly, physiological stimulation of the calyceal input with a SSP increased AP duration to 0.94±0.08ms (n=5). In some cases an initial increase in AP amplitude was observed at early time-points, as would be predicted for a reduction in repolarization conductance. In the presence of 3mM TEA which effectively blocks Kv3 channels, half-widths were 0.71±0.13ms (n=7) and SNP had no additional effect. Inhibition of nNOS with 1400W or of sGC with ODQ blocked the increase in AP duration by SSP or SNP, with half-widths remaining unchanged at 0.47±0.04ms (n=8) and 0.39±0.01ms (n=3), respectively.

Confirmation of the ionic mechanisms of these changes in AP waveform were obtained by using a single-compartment MNTB model incorporating Hodgkin-Huxley type ion channels (see Methods) in which APs were evoked by depolarizing current injection (200-250pA). Block of Kv3 currents was simulated by removal of the high voltage-activated (Kv3) current (Figure 6C, lower left). Interestingly, reproduction of the slowed AP waveform and decreased amplitude caused by NO, required the additional suppression of the voltage-gated Na^+ current by 43% (Figure 6C, top right). Whole-cell patch clamp recordings of voltage-gated Na^+ currents confirmed that NO-donors (SNP and DEA) and delivery of a SSP suppressed the postsynaptic peak voltage-gated Na^+ currents by 37±10% and 50±10%, respectively (Figure S3). Suppression of Na^+ currents was prevented by sGC and nNOS inhibition and was absent in KN2 mice (Gyurko et al., 2002) as shown in Figure S3B. Together these data suggest that NO modulation acts synergistically at multiple sites to modify transmission at this synapse.

The physiological consequences of NO generation, *in vitro* and *in vivo*

The *in vitro* results suggest that modest levels of auditory activity should influence AP firing and hence information transmission across this relay synapse. To test for this, we recorded from mouse MNTB *in vivo* and compared sound-evoked unitary AP waveforms under ketamine anesthesia (in which NMDAR are blocked and nNOS activity suppressed) with equivalent recordings under fentanyl anaesthesia (Figure 6D), an anesthetic which does not block NMDAR. In ketamine-anaesthetized animals sound exposure induced no change in AP waveform. 10-0 min of sound-evoked activity induced a slowing of AP repolarization in fentanyl-anaesthetized mice, which was maintained after ceasing sound exposure. This sound-induced change in AP time course could be blocked by administration of the nNOS antagonist 7-nitroindazole (7-NI, 100mg/kg, *ip*) and potentiated by local ionotophoretic application of Bay 41-2272 (Figure 6D). In one case where pre-spikes (corresponding to calyceal APs) were observed with use of an iontophoretic pipette, application of Bay 41-2272 increased failures of postsynaptic AP firing, consistent with the *in vitro* observations in Figure 7. Similar AP waveforms were obtained for extracellular recordings from single MNTB neurons in slice preparations after SSP application (Figure 6D, right, scaled traces: control in black and SSP in red). A SSP increased AP waveform decay from 0.38±0.11ms to 0.53±0.16ms (n=4, p=0.042, paired Student's t-test). These results are consistent with mediation of sound activity-dependent change in AP waveform through a signaling cascade involving NMDAR, nNOS and sGC to modulate Kv3 currents; as predicted from the *in vitro* data.

To determine the physiological consequences of this NO signaling we examined synaptically evoked 300Hz trains lasting 150ms under current clamp recording conditions (Figure 6E). SNP increased the AP half-widths (Figure 6E) as observed above and reduced transmission rate, as estimated by the number of APs reaching threshold (dotted line). Furthermore, when neurons were stimulated by a SSP, AP half-width increased and transmission started to fail, similar to that seen for application of a NO-donor. These failures were abolished by the NOS inhibitor (1400W, 10μM, Figure 6E), confirming the involvement of endogenous release and action of NO. Thus, the response of the MNTB neuron to the 300Hz stimulation changed from tonic firing to an onset or phasic response and vastly reduced the efficacy of transmission across the calyx of Held/MNTB synapse from 100% transmission (input:output AP) in control conditions to 4.7±1.6% (300Hz train, Figure 6E, bottom graph) following NO signaling.

This change will have a dramatic influence on transmission of information across the MNTB by shifting the output firing from 1:1 following of the presynaptic firing pattern to a phasic onset response. Synaptically evoked trains with Poisson distributed inter-spike intervals (ISI, mean frequency 146Hz) showed mean transmission rates of 82.1±5.5Hz under control conditions (Figure 7A) which decreased to 38.5±7.9Hz on perfusion of SNP (Figure 7A). The frequency histogram (Figure 7B) shows strongly reduced AP firing following ISIs shorter than 21ms, whereas AP firing following longer ISIs was unchanged. In line with the decreased firing frequency, the correlation between the input stimulus train and the output AP train is reduced from 0.47±0.05 to 0.24±0.06 ($p<0.05$, paired Students t-test, n=3) following SNP and measured by the product of spike vectors (Figure 7C, right; see Methods). Identical changes were observed on activating endogenous NO signaling with a SSP stimulation (Figure 7D-F) and this was inhibited by simultaneous perfusion of the nNOS antagonist 1400W (10μM, inset Figure 7E).

Activity-dependent modulation of Kv3 current is absent in a nNOS knockout mouse.
We reasoned that if this activity-dependent signaling were mediated by NO, modulation of Kv3 and AP waveform should be absent in a nNOS knockout mouse. Whole-cell patch recordings were made from 5 MNTB neurons receiving calyceal inputs in brain slices from the KN2 mouse (Gyurko et al., 2002). The synaptic inputs were of similar magnitude to control animals (10.9±1.1nA, -60mV, n=5, not shown). Outward potassium currents were also of similar magnitude to normal animals (Figure 8A, open triangles) and were sensitive to 3mM TEA (data not shown). The outward current was unaffected by delivery of a SSP (open squares) and no change was observed in AP half-width following a SSP (Figure 8B). Furthermore, delivery of short synaptic trains (300Hz, 150ms) always generated postsynaptic APs and this too was unaffected by a prior SSP (Figure 8C). In one case, application of a NO-donor after a negative SSP response, suppressed outward K^+ currents, EPSCs and broaden AP half-width, confirming that down-stream components of the signaling pathway were otherwise intact in the KO animal.

Discussion
These results demonstrate that nitric oxide is an endogenous activity-dependent regulator of neuronal excitability and is predominantly mediated by changes in phosphorylation of postsynaptic Kv3 potassium channels, although several other targets are also involved. The data shows that nNOS is activated by NMDAR at the calyx of Held. NO acts via sGC to raise

cGMP and alters the balance between phosphorylation and dephosphorylation of Kv3 channels: dominance of kinase signaling inhibits Kv3, while supremacy of phosphatase signaling enhances Kv3 currents. Kv3 is closely associated with AP repolarization, so suppression leads to longer APs, more sustained depolarization and inactivation of voltage-gated sodium channels, hence reducing gain and information transmission. The results are consistent with NO acting as a non-classical neurotransmitter or volume transmitter, in that modulation is induced in local inactive neurons by diffusion from adjacent active neurons and suggests that NO signaling scales postsynaptic excitability to changes in synaptic activity across a population of neurons.

There is increasing evidence for non-classical forms of synaptic transmission in the brain (Bullock et al., 2005); ranging from 'spill-over' of neurotransmitter in the synaptic cleft (DiGregorio et al., 2002), to longer-range diffusion, including neuronal-glia interactions, of catecholamine, peptidergic, purinergic and cannabinoid transmitters (Carlson et al., 2002; Fields and Burnstock, 2006). The concept of volume transmission is increasingly recognized as an integral part of brain function (Fuxe et al., 2007). NO is commonly highlighted as possessing the attributes required of a volume transmitter, but the distributed inputs of most excitatory synapses have made this difficult to prove.

Many studies of nitrergic physiology in the brain have focused on changes in synaptic strength, but here we show that this is only part of the mechanism and that postsynaptic excitability changes are also important. NO is acting at multiple sites: locally at glutamate receptors and ionic conductances within the innervated neuron and also by diffusion to adjacent cells. Our data are consistent with tight coupling of NMDAR to nNOS via Ca^{2+} influx, although contributions from Ca^{2+}-permeable AMPAR are possible. There is also a well documented decline in the magnitude of NMDAR currents during maturation at the endbulb and calyx of Held (Bellingham et al., 1998; Futai et al., 2001; Joshi and Wang, 2002). Previously this has been extrapolated to suggest the absence of functional NMDARs at mature brainstem synapses and so it could be argued that coupling to nNOS may be dominated by Ca^{2+}-permeable AMPAR on maturation. However this is incompatible with block of the *in vivo* AP changes by ketamine, and with data from P21 mice, where the SSP-induced DAR-4M fluorescence signals (indicating NO-generation) were completely suppressed by the NMDAR antagonist AP-5 (Figure S4B). Two further observations confirm the primacy of NMDARs in coupling to nNOS: first; although NMDARs decline, they are not eradicated and their slow kinetics means that in terms of conductance (integral) they dominate calyceal AMPARs by 5:1

(Figure S4A) and summate during repetitive stimulation. Second, we have confirmed synaptic NMDAR-mediated currents in P35 mice (Figure S4C) and provided temporal overlap between *in vitro* and *in vivo* recordings from the MNTB for the first time. Finally it might be argued that the NMDARs are functionally inert due to voltage-dependent block by Mg^{2+} at resting membrane potentials. However the SSP and sound-evoked stimuli generate AP trains, each AP will relieve the voltage-dependent block, allowing a pulse of calcium influx (Bollmann et al., 1998; Spruston et al., 1995). Together these results strongly suggest that NMDAR are functionally relevant at mature calyceal synapses and preserve tight coupling to nNOS, presumably through their mutual PDZ binding domains (Kornau et al., 1995). Finally, the *in vivo* data shows that anesthetic doses of ketamine largely suppress NMDAR (Binns and Salt, 1995) and hence NO-signaling.

The broad range of targets raises the possibility that multiple signaling pathways could be involved. We can exclude major contributions from cannabinoid (Kushmerick et al., 2004), metabotropic glutamate receptors (Billups et al., 2005) and A1 adenosine receptors (Wong et al., 2006) since antagonists for these receptors had no effect on Kv3 suppression by a SSP (data not shown). Further evidence supporting predominance of NO signaling is that modulation of Kv3 currents and AP waveforms were absent from the KN2 nNOS knockout mice (Gyurko et al., 2002). The evidence for endogenous NO generation following synaptic stimulation and its action in modulating local and distant neurons constitutes strong evidence that NO is a volume transmitter in the auditory pathway. We postulate that diffusion and summation from multiple sources provides one means of integrating global activity, allowing a slow time-course equilibration between excitability and synaptic transmission across the neuronal population, which would complement cell autonomous mechanisms of synaptic plasticity. This concept is illustrated in Figure 9 in which NO generation by active MNTB neurons summates and modulates excitability across active and inactive cells. Differences in activity rates (including spontaneous firing) across the nucleus could act to adjust the functional tonotopic gradients of intrinsic conductances which have been previously documented (Brew and Forsythe, 2005; Smith et al., 1998; Wang et al., 1998). For instance, the highest spontaneous firing is observed in medial neurons receiving information on high sound frequencies, they exhibit the largest Kv3 currents, but we now predict that they are under the greatest suppression by NO (as illustrated by the NO diffusion model, Figure S1) so the functional Kv3 current *in vivo* will be less than that measured from *in vitro* quiescent slices.

The modulation of both voltage-gated K^+ and Na^+ conductances downstream of activity-dependent NO generation suggests contributions to intrinsic excitability (Daoudal and Debanne, 2003) and/or homeostatic scaling (Marder and Prinz, 2002), with levels of spontaneous activity in the auditory pathway sustaining 'basal' nNOS activity over long periods. Short-term modulation (ms to seconds) at the calyx arises from biophysical phenomena (e.g. facilitation, short-term depression, post-tetanic potentiation and vesicle recycling (von Gersdorff and Borst, 2002), which is highly dependent on the recent history and on-going activity (including spontaneous activity) as recently described by Hermann et al. (2007). This is distinct from the NO-signaling studied here, which has a much slower time-course so that with activation by spontaneous firing, modulation is extended to indefinite time scales. Phosphorylation of Kv3.1b at Ser-503 (Song et al., 2005) is unlikely to mediate this NO-mediated modulation, since this site is not present in mouse kcnc1, but NO-mediated suppression of recombinant Kv3 channels has been observed via a PKG/phosphatase-dependent mechanism (Moreno et al., 2001). These results are of general application since Kv3 K^+ channels and nNOS are broadly expressed throughout the central nervous system and there is significant co-localization; for example, in the hippocampus 86% of nNOS expressing interneurons also express Kv3 subunits (Tansey et al., 2002).

Since brain slices are isolated and inactive for several hours before recording, it seems likely that MNTB basal properties will differ from *in vivo* recordings where neurons are continually exposed to ongoing spontaneous activity. The lack of spontaneous activity *in vitro* means that NO modulation will be low and Kv3 currents larger in these quiescent slices than under physiological conditions. The Poisson-distributed stimulation paradigm shows that high transmission rates (>50Hz) are most strongly suppressed (while onset responses and firing at frequencies below 50Hz are largely unaffected). Transmission failure is consistent with *in vivo* MNTB recordings during sound stimulation where failures are observed (Kopp-Scheinpflug et al., 2003b) and responses to sound show 'primary-like' post-stimulus-time histograms. In terms of brainstem auditory function NO signaling will have little impact on onset responses but will reduce firing rates of MNTB neurons during sustained activity. We do not yet know whether NO modulates cochlear nucleus or upstream nuclei in the SOC and inferior colliculus, so the net effect of NO signaling on hearing may be complex and will require further investigation.

Together, these results show that nitric oxide plays an important role in balancing presynaptic activity with postsynaptic excitability, perhaps serving as a slow gain control mechanism. We

conclude that NO is an activity-dependent volume modulator, adapting intrinsic excitability and synaptic efficacy and modulating both active and inactive neuronal populations to the same physiological input.

Figure 1. nNOS is expressed in postsynaptic MNTB neurons

(**A**)i & ii. Low magnification images of the superior olivary complex at the midline (dashed line) in a transverse section, showing bilateral MNTB nuclei stained with an antibody against Kv3.1b (NeuroMab): scale bars: 100μm. (A)iii. Co-labeling of the section in ii with an eNOS antibody (BD Transduction Lab.) shows high expression in ventral blood vessel and capillaries (*) but no neuronal localization. (A)iv. In contrast, a nNOS antibody (SantaCruz) shows high expression across the MNTB (circled). (**B-D**) i-iii: Scale bars: 20μm. Confocal fluorescence images of MNTB neurons showing co-localization of nNOS (red) with: (**B**) Kv3.1b (green); (**C**) the presynaptic marker vGLUT2 (green, Chemicon) and (**D**) PSD95 (green, AbCam). Merged images include DAPI stained nuclei (blue, iii), and the far right images (iv) show single optical sections from each respective projected confocal image; scale bar: 10μm.

Figure 2. NO and cGMP are generated on stimulation of the calyx of Held

(**A**) Stimulation of the calyceal presynaptic axons in the trapezoid body (100Hz trains for 120s repeated 7 times) increased DAR-4M fluorescence, indicating NO accumulation in neurons possessing a functional calyx (filled squares); less accumulation was observed in neighboring non-connected neurons (open squares); both connected and non-connected neurons increased fluorescence in response to the NO-donor, SNP (800μM). Neurons in control slices receiving no stimulation (open symbols, bottom trace) showed no change in fluorescence. (**B**) Repetition of the two stimulus trains (arrow, SSP=[100Hz trains for 500ms repeated at 1Hz for 60s] x5) showed that each train generated increased NO in connected neurons (n=3), and SNP application further increased the response. (**C**) Fura-2 image of 3 MNTB neurons (380nm ex., left) and DAR-4M fluorescence (560nm ex., middle). Two consecutive SSP trains show raised $[Ca^{2+}]_i$ (red circle & trace, 340/380nm ratio) in the connected neuron but no change in the non-connected MNTB neuron (black circle & trace, 340/380nm ratio). The time course of DAR-4M fluorescence changes ($\Delta F/F_o$) for both cells is plotted (right) for the connected (red) and non-connected (black) neuron showing increased NO with each SSP and for SNP. (**D**) Time-course of DAR-4M fluorescence change following two stimulus trains (SSP1 & SSP2) in the absence (open symbols) or presence (closed symbols) of DNQX (10μM) and AP5 (50μM) during SSP2. (**E**) Summary of the pharmacology for fluorescent detection of NO (filled bars, left axis) and $\Delta[Ca^{2+}]_i$ (open bars, right axis). Bar labeled 'Zero' and dotted line indicate the zero response to SSP2. AP5 (50μM) and DNQX (10μM) reduced NO and $[Ca^{2+}]_i$ accumulation following SSP2. Competitive NOS antagonists L-NMMA (500μM), N-PLA

(10μM) and 1400W (10μM) blocked NO accumulation but not $[Ca^{2+}]_i$ (Ca^{2+} was not measured for L-NMMA), ANOVA, *p<0.05. (**F**) cGMP production in response to synaptic stimulation of the trapezoid body: basal cGMP was increased by phosphodiesterase inhibition (IBMX, 500μM) and massively increased by the NO-donor SNAP (100μM). Calyceal stimulation (SSP) also increased cGMP, with further potentiation by IBMX. Synaptic cGMP accumulation was blocked by N-PLA (10μM) and by blocking AP propagation with tetrodotoxin (1μM). Data are means±SEM, n is indicated within each bar; Student's t test, *p<0.05.

Figure 3. NO is a volume transmitter

(**A**) NO scavenging isolates the NO rise to connected MNTB neurons alone. Images show Fura-2 fluorescence (left) and SSP-evoked NO fluorescence after SSP1 (ΔF_1) & SSP2 (ΔF_2); the NO scavenger PTIO (100μM) was applied prior to SSP2. Neuron receiving a calyceal input (*, red circle and trace, 340/380nm ratio, scale bars: 60s, 0.04a.u.), non-connected neuron (#, black circle and trace, 340/380nm ratio). Line-scan temporal plot (white line on images, far right graph) shows PTIO blocks NO accumulation in the non-connected (black symbols) but not in the connected neuron (red symbols). (**B**) A spatial plot of ΔF_1 along a 100μm line-scan from part A. It shows highest NO accumulation in the connected cell (*) and in the neighboring tissue including the non-connected neuron (#). After PTIO, the ΔF_2 trace (grey) shows reduced fluorescence across the whole slice, except in the connected neuron where synaptic stimulation still induced raised fluorescence. (**C**) Summary graph of NO fluorescence in connected MNTB neurons (On cell) and for 20μm on either side (Off cell) for control (filled bars) and after PTIO (open bars). Student's t test, *p<0.05, means±SEM, n is indicated within the bars. (**D**) The diffusion of NO from connected MNTB neurons is plotted as the change in slope of DAR-4M fluorescence (following an SSP) against distance (diamonds, solid line, n=7). The slope of responses to NO-donor (SNP) perfusion is unchanged with distance (squares, dashed line, n=7). (**E**) Model of NO diffusion from a single 20μm diameter spherical source (located at distance 0) with a production rate of 800nM/sec. Concentration is normalized to the maximum for the 3 conditions (from left to right): 1. NO spread by diffusion, with inactivation. 2. Diffusion with no inactivation. 3. Diffusion and inactivation plus potentiation of NO production as a decaying function of distance from the source centre. Circles show data from part D. (**F&G**) Same image format as part (A) using labeling of single neurons with Fura-2 & DAR-4M. F_0 is control and F_1 is after SSP stimulation for (**F**) two connected neurons and (**G**) one non-connected neuron located adjacent

to two connected neurons. Spatial plots show that NO increases in both cases (F_0 control *vs.* F_1 after SSP, scale bar: 20μm, all images).

Figure 4. NO signaling suppresses Kv3 K^+ currents in connected and non-connected neurons

(**A**) Voltage-clamp of outward K^+ currents for an MNTB neuron receiving a calyceal input; leak subtracted I-V is reduced following an SSP (SSP, open squares); the current recovered after 20min without stimulation (not shown). The inset shows representative raw traces. (**B**) Time-course, the average K^+ current percent amplitude plotted against time for 3-5 connected MNTB neurons (measured at +50mV) following SSP stimulation (arrow, numerals indicate cell numbers). (**C**) Time-course of K^+ current inhibition by DEA-NONOate (100μM) is similar to SSP-induced depression; plot of percent current amplitude (+50mV) against time for control (filled symbols, n=4) and neurons exposed to DEA-NONOate (open symbols, n=6). (**D**) Leak subtracted I-V relationship for a non-connected MNTB neuron (same format as A). A neighboring connected MNTB neuron (<50μm away) was stimulated by a SSP; the K^+ currents are reduced in the non-connected neuron (SSP, open squares). (**E**) Average K^+ current amplitude plotted against time for 3-5 non-connected MNTB neurons (measured at +50mV) following SSP stimulation (arrow, numerals indicate cell numbers). (**F**) Summary plot of absolute K^+ current amplitude (+50mV, leak subtracted) following SSP- and DEA-induced K^+ current depression in connected and non-connected MNTB neurons. (**G**) The I-V relationship for outward K^+ currents (filled diamonds, n = 11) is suppressed following perfusion of SNP (100μM, open triangles). This inhibition was prevented by the sGC inhibitor ODQ (1μM, grey triangles, n=4). Inset shows voltage protocol and raw traces at +50mV with the arrow indicating the measured amplitude plotted in the I-V curve. (**H**) Low concentrations of TEA (3mM) block Kv3 currents (open diamonds, n = 3) after which SNP had no further inhibitory effect (open squares, n=3) confirming that the NO-modulated current is a Kv3 conductance. Inset shows example current traces. (**I**) Summary of K^+ current data shows that SNP dose-dependently reduced Kv3 currents and this was prevented by the sGC antagonist ODQ. The sGC stimulator Bay 41-2272 was without any basal effect. TEA had no additional effect following SNP application. (**J**) PKG antagonist KT5823 enhances control outward currents (open diamonds, n = 3), but the now application of a SSP (filled squares) has no effect, even though Kv3 currents are present until blocked by TEA (3mM, filled triangles, n=3). (**K**) The phosphatase blocker okadaic acid (0.1μM, filled diamonds) mimics the action of NO signaling by suppressing outward potassium currents relative to control currents (filled diamonds, n=3).

(**L**) Summary bar graph shows that KT5823 prevents current suppression by SNP, whereas OA mimics suppression of Kv3 currents. ANOVA for significance, *p<0.05, data denote means±SEM, n is indicated within each bar.

Figure 5. NO reduces synaptic strength by depressing postsynaptic AMPAR and NMDAR

(**A**) Evoked calyceal AMPAR-mediated EPSCs voltage clamped at -60mV, before (black trace) and after NO-donor application (grey trace). (**B**) Voltage clamp at +50mV highlights the slow NMDAR-mediated component, before (black trace) and after NO-donor application (grey trace). (**C**) AMPAR- (filled bars, -60mV) and NMDAR-mediated EPSC (open bar, +50mV) amplitudes are reduced after SNP/DEA (100μM, DEA was used in 2 cases) perfusion or SSP application, which was prevented by nNOS inhibition with 1400W (10μM). Data are expressed as percent control amplitude; with control values being 7.9±1.7nA and 1.8±0.7nA, respectively (n=7). (**D**) EPSC decay time-constants for AMPAR (filled bars) and NMDAR-mediated EPSCs (open bars) were slowed by SNP/DEA or delivery of a SSP and prevented by 1400W (10μM). Paired Student's t test, *p<0.05, n is indicated within each bar. (**E**) Frequency histogram for mEPSC amplitudes (control, black) and after SNP application (red, n=5). Inset shows similar depression of evoked EPSCs and mEPSCs by NO-donors from the same cell. (**F**) Frequency histogram for control decay time-constants of mEPSCs (black bars) and after SNP application (grey bars, n=5). Inset shows the mean amplitude and decay changes for both conditions. Paired Student's t test, n=5, *p<0.05.

Figure 6. NO induces activity-dependent changes of excitability, AP waveform and transmission

(**A**) Suppression of Kv3 currents prolongs AP duration, similar changes were caused by TEA (3mM), SNP (100μM) or a SSP. (**B**) Summary of pharmacological data for AP half-widths. NO donors (SNP & DEA; DEA was used in 4 cases) and TEA slow AP duration. NO-mediated modulation was prevented by ODQ (1μM) but ODQ or Bay 41-2272 (1μM) were without effect when applied alone. Synaptic stimulation (SSP) led to similar increases of AP half-width and this was blocked by 1400W (10μM), ANOVA, *p<0.05. (**C**) Identical AP changes are reproduced in a single-compartment MNTB model incorporating Hodgkin Huxley-type ion channels (see Methods) in response to a depolarising current injection ('control' and 'No Kv3': 200pA, 'NO': 250pA). (**D**) Sound-evoked slowing of AP repolarisation was observed in mouse MNTB *in vivo.* Control unitary AP waveforms (black)

were recorded from mice with anesthetic including fentanyl (left) or ketamine (middle). Following 10-30 minutes of sound exposure, APs decayed more slowly in fentanyl (grey traces), but did not change with ketamine anaesthesia. Right traces show similar slowed AP decay from an *in vitro* MNTB neuron extracellular potential recording before (black) and after SSP (grey). The summary graph shows *in vivo* AP decay times for each of 4 conditions; under control (black bars), at the end of the sound stimulation (grey bars) and immediately following cessation of sound exposure (open bars): (1) fentanyl anesthesia (2) ketamine anesthesia, (3) fentanyl plus NOS antagonist 7-NI (100mg/kg, *ip*) which caused shorter MNTB APs and blocked sound-induced AP changes; (4) activation of local sGC by ionotophoresis of Bay 41-2272 slowed AP decay under control conditions and during sound exposure, ANOVA, *p<0.05. (**E**) Trains of synaptically-induced APs (300 Hz, 150ms) recorded under current-clamp from a MNTB neuron *in vitro* (black trace). NO-donor perfusion (grey trace) and synaptic stimulation (SSP, not shown) caused a failure of APs after the initial stimulus in each train, with only EPSPs remaining (also see Figure 8). The half-width of the first AP was increased by SNP (100μM, grey trace, right inset). The graphs summarize the increase in AP half-width and reduced transmission rate following NO donor application or synaptic stimulation (SSP). The SSP-induced changes were blocked by 1400W (10μM). Data are means±SEM; paired Student's t-test, *p<0.05, n is indicated within each bar.

Figure 7. **NO signaling reduces spike train correlation for pre to postsynaptic transmission**

(**A**) Current clamp from a MNTB neuron receiving a 146Hz synaptic stimulus train with Poisson distributed inter-stimulus intervals (ISI) for control (black) and following SNP application (grey). The lower trace gives an absolute notation of which EPSCs were supra-threshold and generated a postsynaptic AP to the same Poisson train under control (black) and after SNP (grey). (**B**) Frequency histogram of ISIs for control (black) and SNP (100μM, grey) for 3 neurons receiving a 146 Hz Poisson train. (**C**) Left, summary of mean postsynaptic AP frequencies; right, summary of the spike train correlations (normalized dot product, see Methods) for control (black) and on SNP application (grey). (**D**) Current clamp data from a MNTB neuron receiving a 146 Hz synaptic stimulus train with Poisson distributed ISIs for control (black) and after SSP application (grey). (**E**) Frequency histogram of ISI for control (black) and SSP (gray) for 3 neurons. Inset shows histogram for 1 cell incubated with 1400W where a SSP failed to induce failures at higher frequencies. (**F**) Left, summary of mean postsynaptic AP frequencies; right, summary of spike train correlations (normalized dot

product, see Methods) for control (black) and on SSP application (grey). Paired Student's t-test, *p<0.05, means±SEM, n is indicated within each bar.

Figure 8. **Activity-dependent changes are absent in a nNOS knockout mouse**
(**A)** I-V relationship of outward currents in MNTB neurons from nNOS exon 6 knockout (KN2) mice. Synaptic stimulation (SSP) caused no change in high voltage-activated currents. (**B**) Mean half-widths of APs (control, black bars) induced by current injection or by synaptic stimulation (SSP, open bars) are unchanged after a SSP. (**C)** Trains of synaptically-induced APs (300 Hz, 150ms) recorded under current-clamp in a MNTB neuron from a KN2 mouse (Ctrl, upper black trace) is similar to the controls from normal mice, but synaptic stimulation (SSP, lower gray trace) had no effect. (**D**) The first AP of the train for both conditions is superimposed (middle traces) and shows no difference in the half-width following an SSP. The transmission rate was also unaffected by administering a SSP (right bar graph).

Figure 9. NO diffusion and summation across a population of active and inactive neurons
Diffusion of NO from multiple active sources provides modulatory control of synaptic strength and postsynaptic excitability across a population of active and inactive neurons. Three MNTB neurons are shown with highly active calyceal inputs (red), driving these cells to be strong NO sources. This NO can diffuse to influence presynaptic terminals and inactive MNTB neurons in the vicinity. Summation of NO from multiple sources and including spontaneous and evoked activity provides a volume transmission signaling mechanism.

Experimental procedures

In vitro preparations

CBA/CaJ and KN2 (Gyurko et al., 2002) mice aged P10–P35, were killed by decapitation in accordance with the UK Animals (Scientific Procedures) Act 1986 and brainstem slices containing the superior olivary complex (SOC) prepared as previously described (Barnes-Davies and Forsythe). Transverse slices (200µm-thick) containing the MNTB were cut in a low-sodium artificial CSF (aCSF) at ~0°C. Slices were maintained in a normal aCSF at 37°C for 1 hr, after which they were stored at room temperature (~20°C). Composition of the normal aCSF was (mM): NaCl 125, KCl 2.5, $NaHCO_3$ 26, glucose 10, NaH_2PO_4 1.25, sodium pyruvate 2, myo-inositol 3, $CaCl_2$ 2, $MgCl_2$ 1 and ascorbic acid 0.5; L-arginine 0.1; pH was 7.4, bubbled with 95% O_2, 5% CO_2. For the low-sodium aCSF, NaCl was replaced by 250mM sucrose, and $CaCl_2$ and $MgCl_2$ concentrations were changed to 0.1 and 4mM, respectively. All

experiments were carried out at 36±1°C using feedback control of a Peltier device warming the perfusing aCSF (1ml/min).

Electrophysiology

Patch clamp: Whole-cell patch-clamp recordings were made from visually identified MNTB neurons (microscope: Nikon E600FN with DIC optics) using a Multiclamp 700B amplifier and pClamp 9 software (Molecular Devices, Sunnyvale, CA, USA) sampling at 50 kHz and filtering at 10 kHz. Patch pipettes were pulled from borosilicate glass capillaries (GC150F-7.5, OD: 1.5mm; Harvard Apparatus, Edenbridge, UK) using a two-stage vertical puller (PC-10 Narishige, Tokyo, Japan). Their resistance was ~3.0 MΩ when filled with a patch solution containing (mM): KCl 110, HEPES 40, EGTA 0.2, $MgCl_2$ 1, $CaCl_2$ 0.1, Na_2phosphocreatine 5, L-arginine 1; pH was adjusted to 7.2 with KOH and 2mM ATP and 0.5mM GTP was added on the day of use. Whole-cell series resistances were < 12 MΩ, compensated by 70%.

Synaptic stimulation: EPSCs were evoked with a bipolar platinum electrode placed at the midline and using a DS2A isolated stimulator (~3-8 V, 0.2ms; Digitimer, Welwyn Garden City, UK). Synaptic connections were detected using a Fura2 AM (Molecular Probes, Eugene, OR, USA) imaging technique described previously (Billups et al., 2002).

Imaging: was conducted using a PentaMax intensified CCD camera (Princeton Instruments, Inc). The fluorescent image (emission >505nm) was displayed using Metafluor imaging software (Series 7, Molecular Devices), the light source was a Polychrome II Monochromator (TILL Photonics, Martinsried, Germany). For loading of DAR-4M, slices were incubated for 30 min in 5 ml of 10μM DAR-4M AM at room temperature. After loading, slices were post-incubated in aCSF for 30min. and then transferred to the recording chamber. For measurements of NO production, DAR-4M was excited at 560 nm and images acquired every 5 s (exposure time: 20ms) (Mottola et al., 2005). The fluorescence above 575nm was detected using an IF excitation filter, a DM550 dichroic mirror, and a BA575 emission filter (Nikon, Tokyo, Japan).

Radio-immunoassay of cyclic GMP was conducted in identical slices to the electro-physiology and imaging - see Supplementary methods.

***In vivo* recordings:** Spontaneous and evoked responses were recorded from mice (C3HeB/FeJ) MNTB neurons (P17-P70). During the surgical preparation, the animals were anesthetized with a mixture of ketamine hydrochloride (100mg/kg BW) and xylazine hydrochloride (5mg/kg BW). In a subset of experiments, the surgical preparation was done

under ketamine anesthesia while the electrophysiological recordings were performed using a mixture of fentanyl (0.05mg/kg), medetomidin (0.5mg/kg) and xylazine hydrochloride (5mg/kg). Extracellular recordings were made using glasspipettes filled with 3M KCl. MNTB single unit recordings characteristically possess a prepotential, followed by a biphasic postsynaptic action potential and responded to sound from the contralateral ear only (Kopp-Scheinpflug et al., 2003b).

Immunohistochemistry was conducted on 12µm cryostat sections fixed in either methanol or 4 % PFA and processed using standard procedures detailed in the supplementary methods. Antibody sources and details are presented in Supplementary Table 1.

Action potential modeling

A single compartment model of an MNTB principal neuron was constructed using the NEURON simulation software (Carnevale and Lebeda, 1987) by adapting a type II ventral cochlea nucleus cell model (Rothman and Manis, 2003). The MNTB model contained a voltage-gated Na^+ current, a low-voltage activated K^+ current, a high-voltage activated K^+ current (Kv3), a hyperpolarization-activated current (I_h) and a leak current. The magnitudes and reversal potentials of the conductances and the model parameters are given in supplementary Table 2.

Mathematical modeling of NO diffusion: The spread of NO within a block of neural tissue was considered in two different cases: (1) 20µm diameter spherical source of NO located within a large spherical block of tissue and (2) an array of sources in a rectangular slab of tissue. Sources produce NO at a constant rate. NO dissipates by diffusion and is subject to inactivation. Production, diffusion and inactivation rates are as per Hall and Garthwaite (2006). Numerical simulations were carried out in MATLAB, details are in the Supplementary Meth. and source code is available from the author (b.graham@cs.stir.ac.uk).

Data analysis and statistical methods: Results are reported as mean±SEM. Statistical comparison was carried out using Student's *t*-test (paired or unpaired and one- or two-tailed, as indicated) and One way ANOVA was applied when comparing more than 2 data sets. Differences were considered statistically significant at $p<0.05$.

REFERENCES

Ahern, G. P., Klyachko, V. A., and Jackson, M. B. (2002). cGMP and S-nitrosylation: two routes for modulation of neuronal excitability by NO. TINs *25*, 510-517.

Barnes-Davies, M., and Forsythe, I. D. (1995). Pre- and postsynaptic glutamate receptors at a giant excitatory synapse in rat auditory brainstem slices. J Physiol *488,* 387-406.

Bellingham, M. C., Lim, R., and Walmsley, B. (1998). Developmental changes in EPSC quantal size and quantal content at a central glutamatergic synapse in rat. J Physiol *511*, 861-869.

Billups, B. (2005). Colocalization of vesicular glutamate transporters in the rat superior olivary complex. Neurosci Lett *382*, 66-70.

Billups, B., Graham, B. P., Wong, A. Y., and Forsythe, I. D. (2005). Unmasking group III metabotropic glutamate autoreceptor function at excitatory synapses in the rat CNS. J Physiol *565*, 885-896.

Billups, B., Wong, A. Y., and Forsythe, I. D. (2002). Detecting synaptic connections in the medial nucleus of the trapezoid body using calcium imaging. Pflugers Arch *444*, 663-669.

Binns, K. E., and Salt, T. E. (1995). Excitatory amino acid receptors modulate habituation of the response to visual stimulation in the cat superior colliculus. Vis Neurosci *12*, 563-571.

Bogdan, C. (2001). Nitric oxide and the immune response. Nat Immunol *2*, 907-916.

Bollmann, J. H., Helmchen, F., Borst, J. G., and Sakmann, B. (1998). Postsynaptic Ca^{2+} influx mediated by three different pathways during synaptic transmission at a calyx-type synapse. J Neurosci *18*, 10409-10419.

Bon, C. L., and Garthwaite, J. (2003). On the role of nitric oxide in hippocampal long-term potentiation. J Neurosci *23*, 1941-1948.

Bredt, D. S., Hwang, P. M., and Snyder, S. H. (1990). Localization of nitric oxide synthase indicating a neural role for nitric oxide. Nature *347*, 768-770.

Brenman, J. E., Chao, D. S., Gee, S. H., McGee, A. W., Craven, S. E., Santillano, D. R., Wu, Z., Huang, F., Xia, H., Peters, M. F.*, et al.* (1996). Interaction of nitric oxide synthase with the postsynaptic density protein PSD-95 and alpha1-syntrophin mediated by PDZ domains. Cell *84*, 757-767.

Brew, H. M., and Forsythe, I. D. (2005). Systematic variation of potassium current amplitudes across the tonotopic axis of the rat medial nucleus of the trapezoid body. Hear Res *206*, 116-132.

Bullock, T. H., Bennett, M. V., Johnston, D., Josephson, R., Marder, E., and Fields, R. D. (2005). Neuroscience. The neuron doctrine, redux. Science *310*, 791-793.

Carlson, G., Wang, Y., and Alger, B. E. (2002). Endocannabinoids facilitate the induction of LTP in the hippocampus. Nat Neurosci *5*, 723-724.

Carnevale, N. T., and Lebeda, F. J. (1987). Numerical analysis of electrotonus in multicompartmental neuron models. J Neurosci Methods *19*, 69-87.

Daoudal, G., and Debanne, D. (2003). Long-term plasticity of intrinsic excitability: learning rules and mechanisms. Learn Mem *10*, 456-465.

DiGregorio, D. A., Nusser, Z., and Silver, R. A. (2002). Spillover of glutamate onto synaptic AMPA receptors enhances fast transmission at a cerebellar synapse. Neuron *35*, 521-533.

Dodson, P. D., Barker, M. C., and Forsythe, I. D. (2002). Two heteromeric Kv1 potassium channels differentially regulate action potential firing. J Neurosci *22*, 6953-6961.

Elezgarai, I., Diez, J., Puente, N., Azkue, J. J., Benitez, R., Bilbao, A., Knopfel, T., Donate-Oliver, F., and Grandes, P. (2003). Subcellular localization of the voltage-dependent potassium channel Kv3.1b in postnatal and adult rat medial nucleus of the trapezoid body. Neuroscience *118*, 889-898.

Fessenden, J. D., Altschuler, R. A., Seasholtz, A. F., and Schacht, J. (1999). Nitric oxide/cyclic guanosine monophosphate pathway in the peripheral and central auditory system of the rat. J Comp Neurol *404*, 52-63.

Fields, R. D., and Burnstock, G. (2006). Purinergic signalling in neuron-glia interactions. Nat Rev Neurosci *7*, 423-436.

Forsythe, I. D. (1994). Direct patch recording from identified presynaptic terminals mediating glutamatergic EPSCs in the rat CNS, in vitro. J Physiol *479*, 381-387.
Forsythe, I. D., and Westbrook, G. L. (1988). Slow excitatory postsynaptic currents mediated by N-methyl-D-aspartate receptors on cultured mouse central neurones. J Physiol *396*, 515-533.
Futai, K., Okada, M., Matsuyama, K., and Takahashi, T. (2001). High-fidelity transmission acquired via a developmental decrease in NMDA receptor expression at an auditory synapse. J Neurosci *21*, 3342-3349.
Fuxe, K., Dahlstrom, A., Hoistad, M., Marcellino, D., Jansson, A., Rivera, A., Diaz-Cabiale, Z., Jacobsen, K., Tinner-Staines, B., Hagman, B., *et al.* (2007). From the Golgi-Cajal mapping to the transmitter-based characterization of the neuronal networks leading to two modes of brain communication: wiring and volume transmission. Brain Res Rev *55*, 17-54.
Garthwaite, J. (2008). Concepts of neural nitric oxide-mediated transmission. Eur J Neurosci *27*, 2783-2802.
Gyurko, R., Leupen, S., and Huang, P. L. (2002). Deletion of exon 6 of the neuronal nitric oxide synthase gene in mice results in hypogonadism and infertility. Endocrinology *143*, 2767-2774.
Hermann, J., Pecka, M., von Gersdorff, H., Grothe, B., and Klug, A. (2007). Synaptic transmission at the calyx of held under in vivo like activity levels. J Neurophysiol *98*, 807-820.
Hopper, R. A., and Garthwaite, J. (2006). Tonic and phasic nitric oxide signals in hippocampal long-term potentiation. J Neurosci *26*, 11513-11521.
Hurt, K. J., Sezen, S. F., Champion, H. C., Crone, J. K., Palese, M. A., Huang, P. L., Sawa, A., Luo, X., Musicki, B., Snyder, S. H., and Burnett, A. L. (2006). Alternatively spliced neuronal nitric oxide synthase mediates penile erection. Proc Natl Acad Sci USA *103*, 3440-3443.
Ignarro, L. J., Buga, G. M., Wood, K. S., Byrns, R. E., and Chaudhuri, G. (1987). Endothelium-derived relaxing factor produced and released from artery and vein is nitric oxide. Proc Natl Acad Sci USA *84*, 9265-9269.
Jacoby, S., Sims, R. E., and Hartell, N. A. (2001). Nitric oxide is required for the induction and heterosynaptic spread of long-term potentiation in rat cerebellar slices. J Physiol *535*, 825-839.
Joshi, I., Shokralla, S., Titis, P., and Wang, L. Y. (2004). The role of AMPA receptor gating in the development of high-fidelity neurotransmission at the calyx of Held synapse. J Neurosci *24*, 183-196.
Joshi, I., and Wang, L. Y. (2002). Developmental profiles of glutamate receptors and synaptic transmission at a single synapse in the mouse auditory brainstem. J Physiol *540*, 861-873.
Kojima, H., Hirotani, M., Nakatsubo, N., Kikuchi, K., Urano, Y., Higuchi, T., Hirata, Y., and Nagano, T. (2001). Bioimaging of nitric oxide with fluorescent indicators based on the rhodamine chromophore. Anal Chem *73*, 1967-1973.
Kopp-Scheinpflug, C., Fuchs, K., Lippe, W. R., Tempel, B. L., and Rubsamen, R. (2003a). Decreased temporal precision of auditory signaling in Kcna1-null mice: an electrophysiological study in vivo. J Neurosci *23*, 9199-9207.
Kopp-Scheinpflug, C., Lippe, W. R., Dorrscheidt, G. J., and Rubsamen, R. (2003b). The medial nucleus of the trapezoid body in the gerbil is more than a relay: comparison of pre- and postsynaptic activity. J Assoc Res Otolaryngol *4*, 1-23.
Kornau, H. C., Schenker, L. T., Kennedy, M. B., and Seeburg, P. H. (1995). Domain interaction between NMDA receptor subunits and the postsynaptic density protein PSD-95. Science *269*, 1737-1740.
Kushmerick, C., Price, G. D., Taschenberger, H., Puente, N., Renden, R., Wadiche, J. I., Duvoisin, R. M., Grandes, P., and von Gersdorff, H. (2004). Retroinhibition of presynaptic Ca^{2+} currents by endocannabinoids released via postsynaptic mGluR activation at a calyx synapse. J Neurosci *24*, 5955-5965.
Lei, S., Jackson, M. F., Jia, Z., Roder, J., Bai, D., Orser, B. A., and MacDonald, J. F. (2000). Cyclic GMP-dependent feedback inhibition of AMPA receptors is independent of PKG. Nat Neurosci *3*, 559-565.

Lein, E. S., Hawrylycz, M. J., Ao, N., Ayres, M., Bensinger, A., Bernard, A., Boe, A. F., Boguski, M. S., Brockway, K. S., Byrnes, E. J., *et al.* (2007). Genome-wide atlas of gene expression in the adult mouse brain. Nature *445*, 168-176.

Liberman, M. C., and Oliver, M. E. (1984). Morphometry of intracellularly labeled neurons of the auditory nerve: correlations with functional properties. J Comp Neurol *223*, 163-176.

Macica, C. M., von Hehn, C. A., Wang, L. Y., Ho, C. S., Yokoyama, S., Joho, R. H., and Kaczmarek, L. K. (2003). Modulation of the kv3.1b potassium channel isoform adjusts the fidelity of the firing pattern of auditory neurons. J Neurosci *23*, 1133-1141.

Marder, E., and Prinz, A. A. (2002). Modeling stability in neuron and network function: the role of activity in homeostasis. Bioessays *24*, 1145-1154.

Moreno, H., Vega-Saenz de Miera, E., Nadal, M. S., Amarillo, Y., and Rudy, B. (2001). Modulation of Kv3 potassium channels expressed in CHO cells by a nitric oxide-activated phosphatase. J Physiol *530*, 345-358.

Mottola, A., Antoniotti, S., Lovisolo, D., and Munaron, L. (2005). Regulation of noncapacitative calcium entry by arachidonic acid and nitric oxide in endothelial cells. Faseb J *19*, 2075-2077.

Oertel, D. (1999). The role of timing in the brain stem auditory nuclei of vertebrates. Annu Rev Physiol *61*, 497-519.

Palmer, R. M., Ferrige, A. G., and Moncada, S. (1987). Nitric oxide release accounts for the biological activity of endothelium-derived relaxing factor. Nature *327*, 524-526.

Rothman, J. S., and Manis, P. B. (2003). Kinetic analyses of three distinct potassium conductances in ventral cochlear nucleus neurons. J Neurophysiol *89*, 3083-3096.

Rudy, B., and McBain, C. J. (2001). Kv3 channels: voltage-gated K^+ channels designed for high-frequency repetitive firing. TINs *24*, 517-526.

Schneggenburger, R., and Forsythe, I. D. (2006). The calyx of Held. Cell Tissue Res *326*, 311-337.

Smith, P. H., Joris, P. X., and Yin, T. C. (1998). Anatomy and physiology of principal cells of the medial nucleus of the trapezoid body (MNTB) of the cat. J Neurophysiol *79*, 3127-3142.

Son, H., Hawkins, R. D., Martin, K., Kiebler, M., Huang, P. L., Fishman, M. C., and Kandel, E. R. (1996). Long-term potentiation is reduced in mice that are doubly mutant in endothelial and neuronal nitric oxide synthase. Cell *87*, 1015-1023.

Song, P., Yang, Y., Barnes-Davies, M., Bhattacharjee, A., Hamann, M., Forsythe, I. D., Oliver, D. L., and Kaczmarek, L. K. (2005). Acoustic environment determines phosphorylation state of the Kv3.1 potassium channel in auditory neurons. Nat Neurosci *8*, 1335-1342.

Southam, E., and Garthwaite, J. (1993). The nitric oxide-cyclic GMP signalling pathway in rat brain. Neuropharmacology *32*, 1267-1277.

Spruston, N., Jonas, P., and Sakmann, B. (1995). Dendritic glutamate receptor channels in rat hippocampal CA3 and CA1 pyramidal neurons. J Physiol *482*, 325-352.

Tansey, E. P., Chow, A., Rudy, B., and McBain, C. J. (2002). Developmental expression of potassium-channel subunit Kv3.2 within subpopulations of mouse hippocampal inhibitory interneurons. Hippocampus *12*, 137-148.

von Gersdorff, H., and Borst, J. G. (2002). Short-term plasticity at the calyx of Held. Nat Rev Neurosci *3*, 53-64.

Wang, L. Y., Gan, L., Forsythe, I. D., and Kaczmarek, L. K. (1998). Contribution of the Kv3.1 potassium channel to high-frequency firing in mouse auditory neurones. J Physiol *509*, 183-194.

Wang, L. Y., and Kaczmarek, L. K. (1998). High-frequency firing helps replenish the readily releasable pool of synaptic vesicles. Nature *394*, 384-388.

Wong, A. Y., Billups, B., Johnston, J., Evans, R. J., and Forsythe, I. D. (2006). Endogenous activation of adenosine A1 receptors, but not P2X receptors, during high-frequency synaptic transmission at the calyx of Held. J Neurophysiol *95*, 3336-3342.

Supplementary Figures & Methods

Nitric oxide is a volume transmitter regulating postsynaptic excitability at a glutamatergic synapse

By Joern R. Steinert, Cornelia Kopp-Scheinpflug, Claire Baker, R.A. John Challiss, Raj Mistry, Martin D. Haustein, Sarah J. Griffin, Huaxia Tong, Bruce P. Graham, Ian D. Forsythe.

Table 1: Antibodies used in this study.

BP-blocking peptide, Ab-antibodies used for figures in **bold**

We have used well characterised antibodies for which there are published images available. Where available, blocking peptide (BP) controls have been conducted and in each case it blocked staining by the primary Ab (not shown) as noted in Table 1. We have confirmed similar staining of Kv3.1 in the MNTB by both Alomone and NeuroMab Abs. Co-localisation images were taken using Abs raised in different hosts.

Protein	**Host**	**BP used**	**Ab used from different sources**	**Reference**
Kv3	rabbit mouse	yes	**Alomone**; **NeuroMab**	(Dodson et al., 2003)
nNOS	rabbit mouse	yes yes	**Santa Cruz**; BD Transduction Lab	(Buchwalow et al., 2005; Dietz et al., 2005)
eNOS	mouse	no	**BD Transduction Lab**	(Cao et al., 2001)
vGLUT2	guinea pig	yes	**Chemicon**	(Billups, 2005)
PSD 95	mouse	no	**Abcam**	(Kornau et al., 1995)

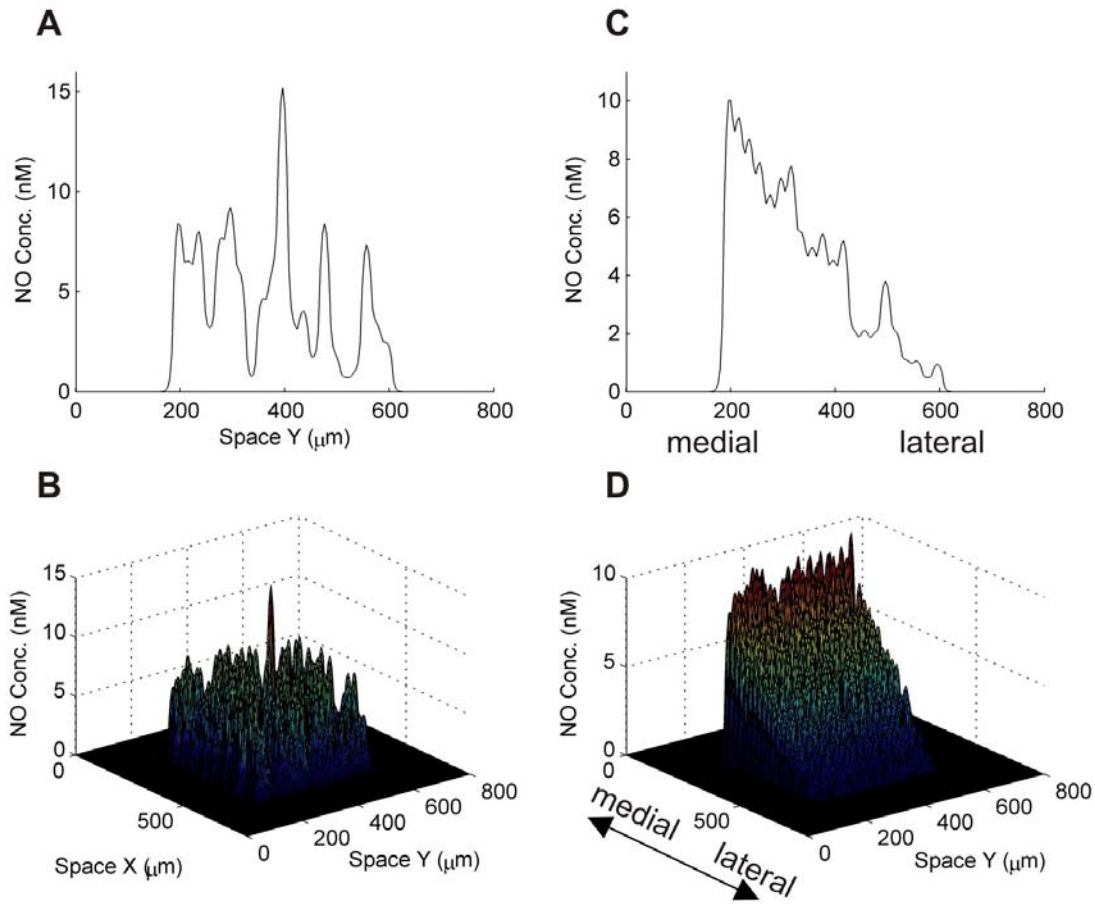

Figure S1. Mathematical modelling of the spread of NO

A, Model of NO concentration gradients produced by a 21 by 21 tightly-packed planar array of 20μm diameter spherical sources embedded in a block of neural tissue. Each source is assigned a production rate drawn randomly from a range of 0 to 1600nM/s. The central source is assigned an elevated rate of 2400nM/s to simulate a single activity-driven input. Simulations run for 100ms, which is sufficient to achieve a steady [NO] profile. **B**, 3-D representation of the same data. **C**, Using similar NO production rates which decrease linearly from 1600nM/s at the left (medial) edge of the cell array to 16nM/s at the right (lateral) edge, consistent with trends of spontaneous activity across the tonotopic axis. **D**, 3-D representation of the same data.

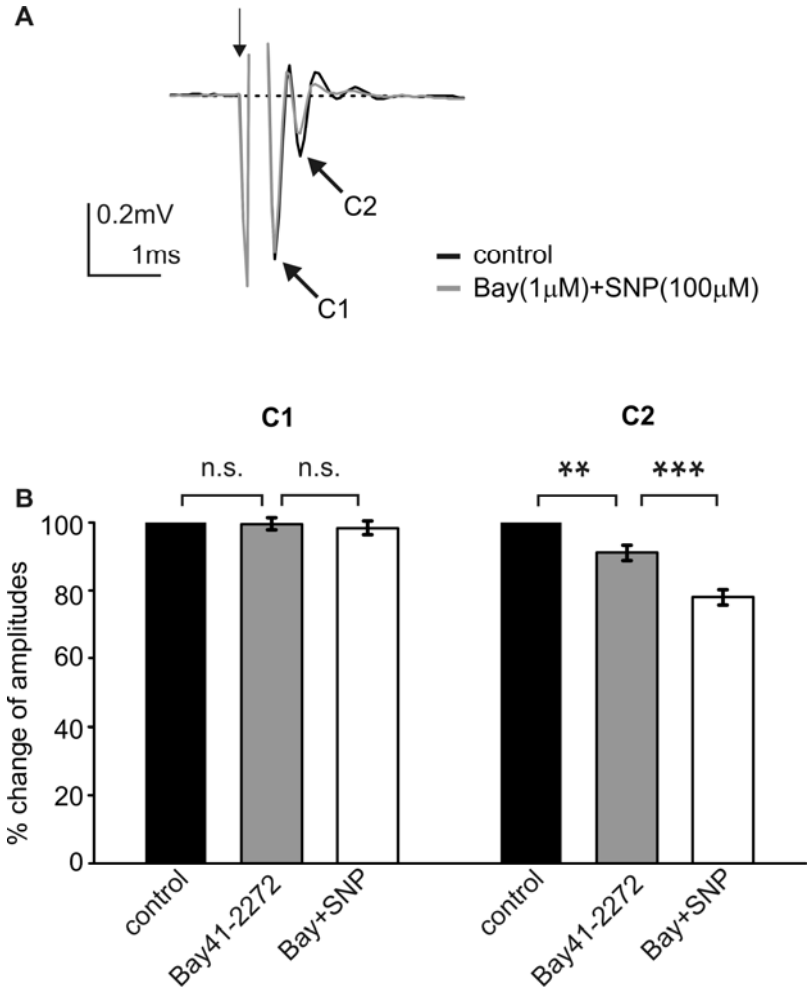

Figure S2. Effect of Bay 41-2272 and SNP on extracellular fieldpotentials recorded by multielectrode arrays in the MNTB

A, Example traces of a typical extracellular field potential recording of MNTB neurons by a multielectrode (MED64; Alpha MED Sciences, Japan) array before (black trace) and after (grey trace) application of Bay 41-2272 (1μM) and SNP (100μM). Traces show that the presynaptic response (C1) is unaffected, whereas the postsynaptic component (C2) is reduced in amplitude.

The stimulus artifact (indicated by arrow) is cut off for clarity. **B**, Summary of MED data obtained from 19 electrodes of 4 brainslices from 4 Lister hooded rats (P16-17). The C1 components show no statistically significant change in amplitude but the C2 component is reduced in the presence of Bay 41-2272 and SNP. All recordings were obtained at 36°C. *$p<0.05$, paired Student's t-test was used to test for statistical significance.

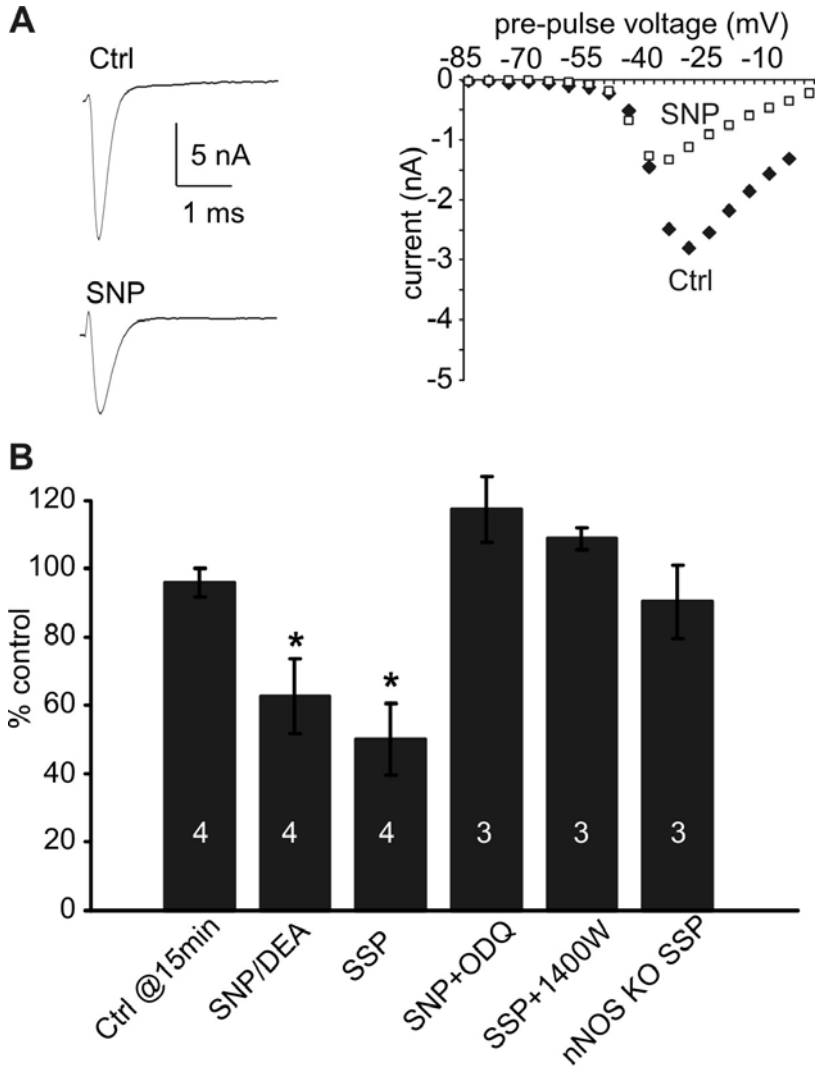

Figure S3. NO and synaptic activity reduce sodium currents

A, sample traces for sodium currents under control conditions and on SNP application and a representative I-V relationship for both conditions. **B**, Summary of Na^+ currents expressed as percent control for control recordings 15 min after initial whole cell recording, SNP/DEA (100μM, DEA was used in 2 cases) and SSP. The presence of ODQ (1μM) eliminated the effect of SNP and incubation with 1400W (10μM) prevented Na^+ depression after SSP. Likewise, a SSP had no effect on Na^+ currents in nNOS KO (KN2) mice. ANOVA for significance, *$p<0.05$, data denote means±SEM, n is indicated within each bar. Asterisks indicate statistical significance from control.

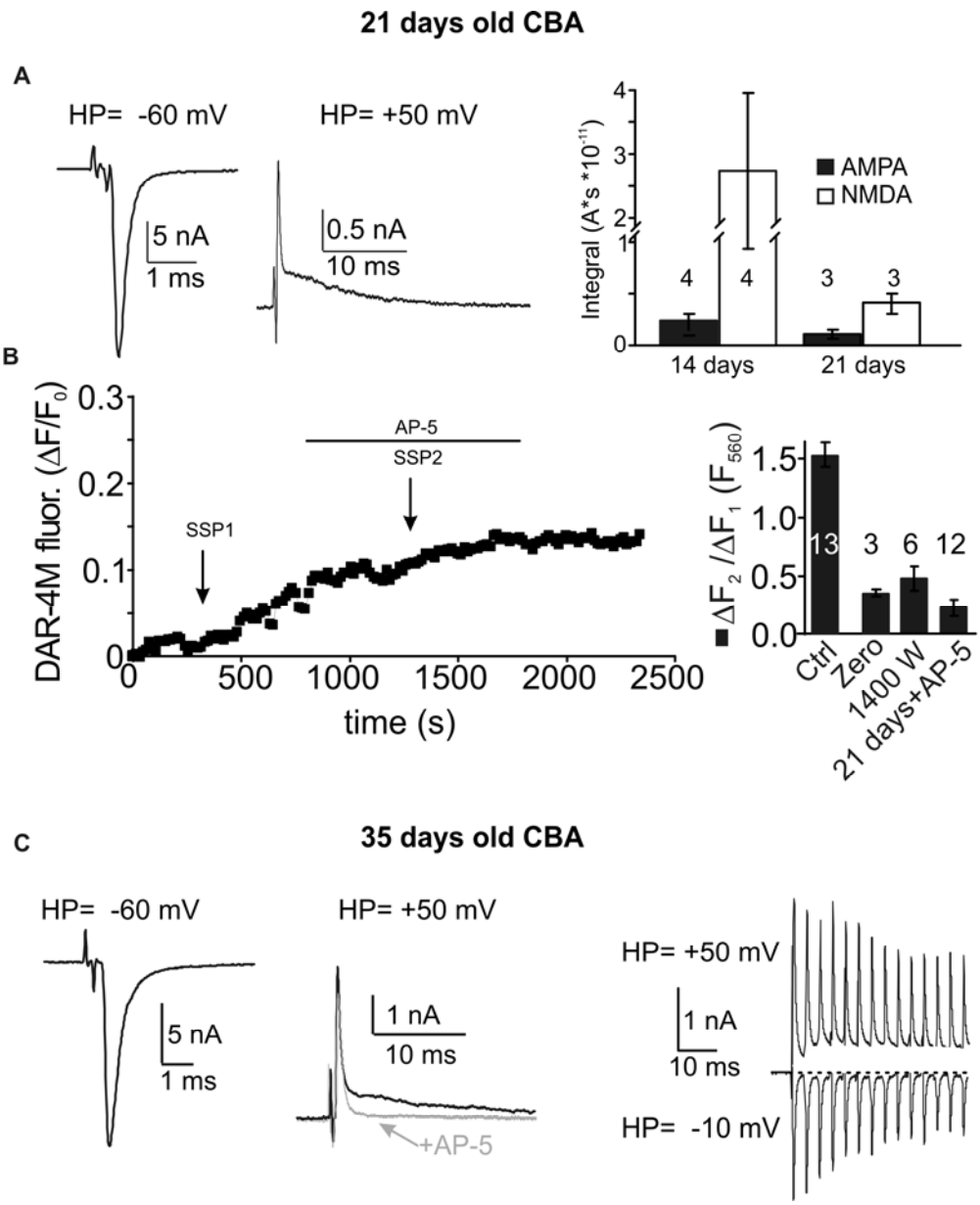

Figure S4. NMDAR currents in MNTB neurons from P21 and P35 CBA mice.

A, Calyceal EPSCs from P21 CBA mice. Left, representative EPSC traces are shown for holding potentials (HP) of -60mV and +50mV. Right, the calculated integral for AMPA and NMDA currents at 14 and 21 days. **B**, NO-imaging from P21 CBA mice. DAR-4M fluorescence increases following synaptic stimulation (SSP1). AP-5 suppresses the fluorescence change induced by SSP2. Right, summary graph of $\Delta F_2/\Delta F_1$ ratios shows the effects of AP-5 in MNTB neurons. Compare data with figure 2 for data from younger animals. **C**, Calyceal EPSCs from P35 CBA mice. EPSC traces are shown for holding potentials (HP) of -60mV (left) and +50mV (middle). Currents from two MNTB neurons are overlaid. A slow outward current mediated by NMDAR is present in the control neuron. Repetitive stimulation causes summation of these small NMDA currents, as shown on the right; with overlaid responses to 300Hz train at HP of +50 mV and -10 mV.

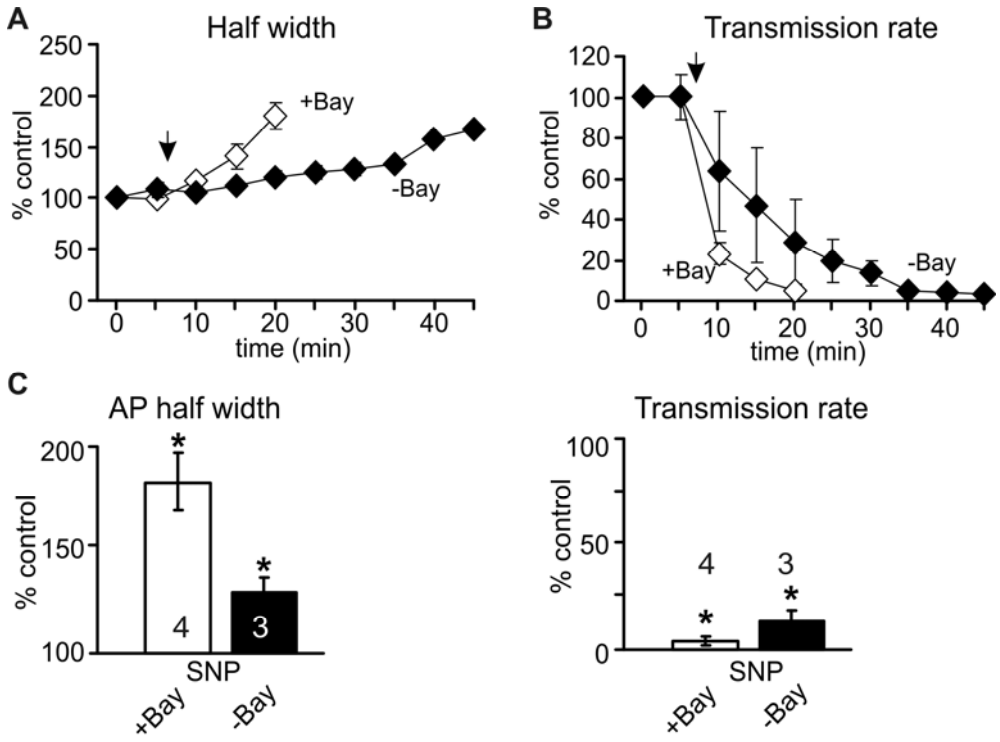

Figure S5. In the absence of Bay 41-2272, the response to NO has a slower time-course, but is otherwise similar to that in the presence of 1 μM Bay 41-2272

Because the response to NO is slow, even at 37^{o}C, many electrophysiology experiments were performed in the presence of Bay 41-2272. **A**, Time course of change in action potential half-width in the absence (filled squares, n=3) or presence (open squares, n=4) of Bay 41-2272. Arrow indicates application of SNP (100μM). **B**, Time course of the change in transmission rate of synaptically-evoked action potentials within a 300 Hz, 200ms train for the absence (filled squares, n=3) and presence (open squares, n=4) of Bay 41-2272. Arrow indicates application of SNP (100μM). Data denote means±SEM. **C**, Summary data showing increase in half-width and transmission rates with and without Bay 41-2272.

Supplementary Methods

***In vitro* preparations.**

Transverse brain slices were prepared from 10-35 day old CBA/CaJ mice or from homozygous KN2 nNOS knockouts (Gyurko et al., 2002) obtained from colonies maintained at the University of Leicester. Animals were killed by decapitation according to approved methods under the UK government Animal Scientific Procedures Act 1986. The head was then cooled in iced low sodium aCSF and rapidly removed from the skull. A tissue block containing the brainstem was glued onto the stage of a Campden Instuments IntegraSlice and transverse sections (thickness 200 μm) cut of the superior olivary complex. The slices were placed in a gassed (95%O_2/5%CO_2) re-circulating chamber containing normal aCSF (see main methods for composition) and maintained at about 36^{o}C for one hour, after which they slowly cooled to room temperature. For all patch and imaging experiments one slice was placed in an environmental chamber on the stage of the microscope (Nikon E600FN fitted with differential interference contrast optics) and maintained by perfusion of aCSF at a rate of 1ml/min and temperature of 36^{o}C. Whole-cell patch recordings and imaging experiments were made on visually identified MNTB neurons. Patch pipettes were pulled from borosilicate glass capillaries (GC150F-7.5, OD: 1.5mm; Harvard Apparatus, Edenbridge, UK) using a two-stage vertical puller (PC-10 Narishige, Tokyo, Japan). Their resistance was ~3.0 MΩ when filled with a patch solution containing (mM): KCl 110, HEPES 40, EGTA 0.2, $MgCl_2$ 1, $CaCl_2$ 0.1, Na_2phosphocreatine 5, L-arginine 1; pH was adjusted to 7.2 with KOH and 2mM ATP and 0.5mM GTP was added on the day of use. Whole-cell series resistances were < 12 MΩ and recordings in which the series resistance changed by more than 20% were eliminated from analysis. Lags of 10 μsec were used with series resistance prediction and compensation set to 70%. Leak subtraction was not employed for I/V plots except in figure parts 4A, 4D and S3A. A junction potential of -3 mV was not compensated. Two factors seemed crucial for observation of endogenous NO production and Kv3 modulation: first, experiments were conducted at 36^{o}C, whereas recordings at room temperature showed little change (data not shown). Second, the observed changes generally had a slow onset, so requiring 15-30 minutes of stable recording, with minimal change in series resistance (see use of Bay 41-2722, below and Figure S5).

For recording extracellular unitary action potentials, MNTB neurons were 'loose patched' with seal resistances of 50 - 100MΩ. Pipettes contained extracellular aCSF and had a resistance of ~3MΩ. Action potentials were evoked by presynaptic stimulation of the trapezoid body at the midline.

Synaptic stimulation: EPSCs were evoked with a bipolar platinum electrode placed across the slice on the trapezoid body axons at the midline and using a DS2A isolated stimulator (~3-8 V, 0.2ms; Digitimer, Welwyn Garden City, UK). Calyceal synaptic connections were detected using a Fura2 AM (Molecular Probes, Eugene, OR, USA) imaging technique described previously (Billups et al., 2002). Stimulation of non-calyceal excitatory inputs to MNTB neurones was minimised, since they require higher stimulus intensities (Hamann et al., 2003). Calyceal EPSCs were recorded in the presence of strychnine (1μM) and bicuculline (10μM) and in some cases included QX314 (5mM) in the patch pipette to suppress voltage-gated sodium currents. The synaptic stimulation protocol (SSP) is an average 50Hz stimulation over one minute (stimulation 100Hz, 500ms on, 500ms off, repeated at 1Hz for 60s) thereby providing a repeatable protocol for pharmacological studies.

Use of Bay 41-2722. Because of the slow time-course of the NO modulation, low concentrations of Bay 41-2722 (1 μM) were routinely used for the electrophysiological experiments (Hopper and Garthwaite, 2006) to accelerate the signaling time-course. In experiments without Bay 41-2722, identical changes were observed but their time-course was 2 to 3 times slower (30-40 min) in onset (Figure S5). Bay 41-2722 was not used for the imaging or cGMP production experiments.

Intracellular Imaging

Calcium: Slices were loaded with 5 μM Fura 2 AM (Molecular Probes, Eugene, OR, USA, dissolved in DMSO containing 5% pluronic acid) for 5 min in aCSF. Before recording, slices were kept in aCSF for 30 min to allow de-esterification of the AM dye. Fura 2 fluorescence was detected using imaging technique described previously (Billups, 2005) and viewed using a PentaMax intensified CCD camera (Princeton Instruments, Inc). The fluorescent image (emission >505nm) was displayed using Metafluor imaging software (Series 7, Molecular Devices), the light source was a Polychrome II Monochromator (TILL Photonics, Martinsried, Germany).

DAR4-M: Loading of whole slices required incubation for 30 min in 5 ml of 10μM DAR-4M AM at room temperature in gassed aCSF in a conical tube mounted on a oscillating table to provide perturbation. After loading, slices were post-incubated in aCSF for 30 min. and then transferred to the recording chamber. For measurements of NO production, DAR-4M was excited at 560 nm and images acquired every 5 s (exposure time: 20ms) (Mottola et al., 2005).

The fluorescence above 575 nm was detected using an IF excitation filter, a DM550 dichroic mirror, and a BA575 emission filter (Nikon, Tokyo, Japan). Single MNTB neurons were loaded for 10 min with a pipette in loose patch configuration (pipette resistance was ~2MΩ) filled with 50 μM DAR-4M AM in aCSF at 35-36^{o}C. Before recording cells were perfused with gassed aCSF for 15 min at 36^{o}C. Methodological notes: There is clear evidence that NO is required for DAR-4M fluorescence changes in tissue samples and the response in the MNTB is sensitive to nNOS antagonists, however the fluorescence may be influenced by other nitrergic species and the reaction with NO is irreversible. With these caveats, the DAR-4M fluorescence gives a qualitative indication of NO generation. Scavenging of NO was achieved by extracellular perfusion of PTIO, which may not be excluded from intracellular compartments as effectively as the carboxy-PTIO, but access of PTIO into the cell does not affect interpretation of its action in NO scavenging.

Radio-immunoassay of cyclic GMP

Control, NO-donor stimulation (SNAP, 100 μM, 10 min) or midline-SSP stimulated brain slices (see above) were used for assessing synaptically-induced cGMP production. Briefly, the SOC was isolated and neutralized tissue extracts were diluted five-fold in 100mM sodium acetate, pH 6.2 and acetylated by consecutive addition of triethylamine (10μl) and acetic anhydride (5μl) and used in the radioimmunoassay (Brooker et al., 1979) within 60 min. Cyclic GMP standards (100μl; 0-4nM) were treated identically. Acetylated samples (100μl) were mixed with 2'-*O*-succinyl 3-[^{125}I]-iodotyrosine methyl ester cyclic GMP (GE Healthcare, IM107) (50μl, ~3,000 d.p.m. made up in 50mM sodium acetate, 0.2% bovine serum albumin (BSA), pH 6.2) and 100μl of anti-cyclic GMP antibody (GE Healthcare, TRK500; diluted in 50mM sodium acetate, 0.2% BSA, pH 6.2). Samples were intermittently vortex-mixed during a 4 h incubation at 4^{o}C. Free and bound cyclic GMP was separated by charcoal precipitation with 500μl of a charcoal suspension (1% (w/v) activated charcoal in 100mM potassium phosphate, 0.2% BSA, pH 6.2). After vortex-mixing for 5 min samples were centrifuged (13,000 g, 4 min, 4^{o}C) and radioactivity determined in an aliquot of supernatant (600μl). Unknown values were determined from the cyclic GMP standard curve using GraphPad Prism 4 (GraphPad Software Inc., San Diego, CA).

Extracellular MED64 recordings

Recordings were made on Multi-electrode devices (MED64; Alpha MED Sciences, Japan) on brainstem slices of Lister Hooded rats (P13-P16) containing the superior olivary complex, prepared as previously described (Song et al., 2005; Wong et al., 2003) and using identical

methods to those for preparation of mouse brainstem slices. One slice was transferred onto a microscope where a MED64 probe and a MED64 connector were positioned, aCSF was perfused and pre-heated at 36^{o}C. Several channels of data were recorded at a sampling rate of 20 kHz with 12-bit resolution. A field excitatory postsynaptic potential (fEPSP) was evoked via stimulation at one MED64 electrode at the midline by a biphasic stimulus (±100 μA, 160 μs). fEPSPs were recorded for up to 60 min with MED64 Conductor software. The amplitude of fEPSP was measured from baseline to the negative peak. Data were compared as a percentage change.

***In vivo* extracellular recordings**

Preparation: Spontaneous and evoked responses were recorded from mice (C3HeB/FeJ) MNTB neurons (P17-P70). During the surgical preparation, the animals were anesthetized with a mixture of ketamine hydrochloride (100 mg/kg BW) and xylazine hydrochloride (5 mg/kg BW). In a subset of experiments, the surgical preparation was done under ketamine anesthesia while the electrophysiological recordings were performed using a mixture of fentanyl (0.05 mg/kg), medetomidin (0.5 mg/kg) and xylazine hydrochloride (5 mg/kg). The skull of was exposed along the dorsal midsagittal line. Two holes were drilled in the skull 2000-2300 μm caudal to the lambda suture. The first drill hole, located 1500 μm lateral to the midline, was used to position the reference electrode in the superficial cerebellum. For the insertion of recording electrodes the second drill hole (500 μm diameter) was located over the midline, and the electrodes were angled at 5°-8° to the midsagittal plane. The recording site was verified histologically using HRP marking (Kopp-Scheinpflug et al., 2003).

Recording: Experiments were conducted on 30 MNTB neurons from 6 animals contributing a total pool of analyzed spontaneous and evoked APs in excess of 327,000 events. Recordings were made using glass micropipettes (15-30 MΩ, 3M KCl). The electrode was advanced vertically by a motorized micromanipulator (WPI, DC3001). Single units were identified by their relatively constant spike height and characterized by complex spike waveforms, which consists of a monophasic positive potential (prepotential) followed by a biphasic action potential and responded only to sound stimulation of the contralateral ear. The activity of isolated single units was filtered (0.3-10 kHz) and amplified (TDT, PC1) to the voltage range of the spike discriminator (TDT, SD1) and recorded at 100 kHz using custom-written software (Dr. M. Weick, University of Leipzig; Weaver, B. Englitz, MPI Mathematics in the Sciences, Leipzig).

Stimulus and recording protocols: Stimulus tones (100ms duration, 5ms rise-fall time, 100 ms inter-stimulus interval) were generated at a 50 kHz sampling rate using (TDT; RP2-1),

amplified (TDT; ED1), delivered to electrostatic speakers (TDT; EC1) and fed via acoustic tubing to the outer ear approximately 5 mm from the animal's eardrum. For each neuron the following stimulation protocol was employed: 3 min of spontaneous firing, determination of CF and threshold, 5 to 30 min of CF-stimulation at 80 dB SPL and again followed by 3 min of spontaneous firing.

Drug application

In vitro, drugs were applied by bath perfusion in aCSF.

In vivo 7-Nitroindazole (7-NI) was dissolved in sesame oil and administrated via *ip* injection at a dose of 100mg/kg. Bay 41-2272 was dissolved in saline as a 10 μM solution and administered by iontophoresis from a separate 'piggy-back' pipette.

Drugs were obtained from: AP-5 (Tocris, UK), 6,7-dinitroquinoxaline-2, 3-dione (DNQX, Tocris, UK), TEA (SIGMA), N^{ω}-Propyl-L-arginine (N-PLA, SIGMA), 1400W (SIGMA), L-NMMA (SIGMA), ODQ (Calbiochem), KT5823 (SIGMA), okadaic acid (SIGMA), IBMX (Calbiochem), TTX (Tocris), Bay41-2272 (Calbiochem), SNAP (Calbiochem), SNP (Calbiochem), Diethylamine NONOate (DEA NONOate, Calbiochem), DAR-4M AM (Calbiochem) and PTIO (Calbiochem). SNP and DEA NONOate were made up on the day of use immediately prior to the experiment and kept on ice. Other drugs were dissolved as stock solutions in water or DMSO, aliquoted and frozen at -20°C and diluted in aCSF immediately before the experiment. Low concentrations of SNP, SNAP or DEA were used to minimize nitrosylation and peroxynitrite formation.

Immunohistochemistry

Brains were frozen in Tissue-Tek OCT compound (Sakura) and cryostat sectioned at 12 μm in the transverse plane. Sections were fixed in either Methanol at -20^{o}C or 4% paraformaldehyde at 4^{o}C and subsequently incubated for 30 mins at room temperature with PBS containing 0.1% Triton X-100 (PBS-T), 1% BSA and 10% normal goat serum (NGS) to reduce non-specific binding of secondary antibody. Sections were incubated with primary antibodies to nNOS (1:1000, SantaCruz), eNOS (1:1000, BD Transduction Lab.), vGLUT2 (1:1000, Chemicon), PSD95 (1:1000, AbCam) and/or Kv3.1b (1:1000, NeuroMab) diluted in PBS-T containing 1% BSA and 10% NGS overnight at 4^{o}C. After three washes in PBS-T, sections were incubated with the secondary antibodies (Invitrogen) diluted in PBS-T, 1% BSA and 10% NGS for 2 hours at room temperature. AlexaFluor 546 goat anti-rabbit IgG (1:1000) was used to recognize nNOS/NOS1, AlexaFluor 488 goat anti-guineapig IgG (1:1000) to recognize vGLUT2 and AlexaFluor 488 goat anti-mouse IgG (1:500) to recognize Kv3.1b. After rinsing

in PBS-T, sections were cover-slipped with Vectashield Hard Set Mounting Medium with DAPI (Vector Laboratories) and images were acquired with a Zeiss laser-scanning confocal microscope (LSM 510, Carl Zeiss International) or Leica DM2500 fluorescence microscope. As negative controls for specificity, sections incubated with the omission of the primary antibody showed no specific immunostaining (data not shown) and pre-incubation with antigenic peptide (where available) also blocked specific staining. Details for the antibodies are summarized in supplementary Table 1.

Modelling

A single compartment model of an MNTB principal neuron was constructed using the NEURON simulation software (Carnevale and Lebeda, 1987) by adapting a type II ventral cochlea nucleus cell model (Rothman and Manis, 2003). The MNTB model (run at a simulated temperature of 37^{o}C) contained a voltage-gated Na^+ current, a low-voltage activated K^+ current (LVA), a high-voltage activated K^+ current (HVA), a hyperpolarization-activated current (I_h) and a leak current. The magnitudes and reversal potentials of the conductances and the parameters of the additional K^+ current are given in Table 2 (below). Block of Kv3 K^+ current was simulated by a 60% reduction in the high-voltage-activated K^+ current; simulation of the NO effect required an additional 43% reduction in the magnitude of the model Na^+ conductance.

Table 2: Conductance values for HH model of MNTB neurons (Figure 6C)

Based on a Rothman and Manis (2003) Bushy cell model at 37^{o}C

	Magnitude nS	E_{Rev} mV
Leak	7	-67
Na (control)	800	50
Na (NO)	450	50
LVA	20	-70
HVA (control)	120	-70
HVA (TEA and NO)	48	-70
Ih	6	-43

Mathematical modeling of the spread of NO (Figure 3E and Figure S1)

Single spherical source

The situation of diffusion from a single spherical source of NO is radially symmetric and is modeled using one radial dimension from the centre point of the source:

$$\frac{\partial[NO]}{\partial t} = D\left(\frac{\partial^2[NO]}{\partial r^2} + \frac{2}{r}\frac{\partial[NO]}{\partial r}\right) + P - I$$

where [NO] is the nitric oxide concentration at radial distance *r* from the centre of the spherical source. *D* is the diffusion constant. *P* is the NO synthesis rate, which is set to fixed value P_0 within the spherical source. *I* is the rate of NO inactivation (Hall and Garthwaite, 2006):

$$I = \frac{V_{\max}[NO]}{K_m + [NO]}$$

The radial diffusion equation was solved using the *pdepe* function in MATLAB. Boundary conditions are that the [NO] spatial gradient is zero for *r*=0 and *r*=*l*, where *l* is the maximum radial length (here usually set to 200μm) from the centre of the source at *r*=0. Calculations were done using a spatial step of 0.5μm, with the time step being chosen by *pdepe*. Parameter values were set to: D=3300μm^2/sec, P_0=800nM/sec, V_{max} =2000nM/sec, K_m=10nM. Potentiation of NO production was modeled as a decaying function of distance *x* (in μm) from the spherical source, with:

$$P = \frac{P_0}{1 + \exp(0.05(x - 100))}$$

The coefficients were chosen to provide an empirical fit to the NO imaging data.

Array of sources

To handle distributed sources of NO in a block of tissue it is necessary to use a finite difference method to calculate NO on a three-dimensional grid of spatial points (Philippides et al., 2005). The three dimensional diffusion equation is given by:

$$\frac{\partial[NO]}{\partial t} = D\left(\frac{\partial^2[NO]}{\partial x^2} + \frac{\partial^2[NO]}{\partial y^2} + \frac{\partial^2[NO]}{\partial z^2}\right) + P - I$$

This was solved numerically using an alternating direction implicit (ADI) finite difference method written in MATLAB. Boundary conditions are again that spatial gradients at the edges are zero. The spatial step is 4μm to allow reasonable spatial resolution while being able to simulate a large tissue block (200x200x100 spatial grid points corresponding to an 800x800x400μm block.) When inactivation is included a time step of 1msec is used to ensure stability. Without inactivation a time step of 40msecs is sufficient and allows simulation of longer time courses in a reasonable computation time.

A two-dimensional array in the x-y plane of 441 (21 by 21) 20μm spherical sources of NO is embedded within the middle of the tissue block, such that the centre of the source in the middle of the array is located at x-y-z coordinates (400,400,200)μm. All sources are centered

at 200μm in the z (vertical) direction, but vary in their x and y coordinates. The array is tightly packed such that the distance between source centers is 20μm.

Diffusion and inactivation parameters are as for a single spherical source. Each source in the array is assigned its own constant production rate *P*. NO production is set to zero outside of the sources.

Correlation of spike trains: Presynaptic stimulation *vs.* postsynaptic AP firing (Figure 7C, F)

To compare input and output spike trains, action potential times were collected (measured as the time of peak membrane potential for each AP waveform) from individual trains. Binary vectors were generated using a bin size of 2 ms by entering '1' in each bin in which an AP had occurred. The first bin corresponded to the first spike, providing synchronization between the stimulus and the MNTB trains that compensates for synaptic delay. A correlation was then calculated as the inner product of a stimulus and MNTB (output) spike vector, which effectively counts the spikes in common between the two vectors, normalized against the inner product of the stimulus vector itself.

References

Billups, B. (2005). Colocalization of vesicular glutamate transporters in the rat superior olivary complex. Neurosci Lett *382*, 66-70.

Brooker, G., Harper, J. F., Terasaki, W. L., and Moylan, R. D. (1979). Radioimmunoassay of cyclic AMP and cyclic GMP. Adv Cyclic Nucleotide Res *10*, 1-33.

Buchwalow, I. B., Minin, E. A., Samoilova, V. E., Boecker, W., Wellner, M., Schmitz, W., Neumann, J., and Punkt, K. (2005). Compartmentalization of NO signaling cascade in skeletal muscles. Biochem Biophys Res Commun *330*, 615-621.

Cao, S., Yao, J., McCabe, T. J., Yao, Q., Katusic, Z. S., Sessa, W. C., and Shah, V. (2001). Direct interaction between endothelial nitric-oxide synthase and dynamin-2. Implications for nitric-oxide synthase function. J Biol Chem *276*, 14249-14256.

Carnevale, N. T., and Lebeda, F. J. (1987). Numerical analysis of electrotonus in multicompartmental neuron models. J Neurosci Methods *19*, 69-87.

Dietz, G. P., Schott, M., Labes, M., and Bahr, M. (2005). Expression of the protein inhibitor of nitric oxide synthase in the adult rat retina before and after optic nerve lesion. Brain Res Mol Brain Res *136*, 118-124.

Dodson, P. D., Billups, B., Rusznak, Z., Szucs, G., Barker, M. C., and Forsythe, I. D. (2003). Presynaptic rat Kv1.2 channels suppress synaptic terminal hyperexcitability following action potential invasion. J Physiol *550*, 27-33.

Hall, C. N., and Garthwaite, J. (2006). Inactivation of nitric oxide by rat cerebellar slices. J Physiol *577*, 549-567.

Hamann, M., Billups, B. and Forsythe, I.D. (2003) Non-calyceal excitatory inputs mediate low fidelity synaptic transmission in rat auditory brainstem slices. Eur. J. Neuroscience 18: 2899-2902.

Hopper, R. A., and Garthwaite, J. (2006). Tonic and phasic nitric oxide signals in hippocampal long-term potentiation. J Neurosci *26*, 11513-11521.

Kopp-Scheinpflug, C., Lippe, W. R., Dorrscheidt, G. J., and Rubsamen, R. (2003). The medial nucleus of the trapezoid body in the gerbil is more than a relay: comparison of pre- and postsynaptic activity. J Assoc Res Otolaryngol *4*, 1-23.

Kornau, H. C., Schenker, L. T., Kennedy, M. B., and Seeburg, P. H. (1995). Domain interaction between NMDA receptor subunits and the postsynaptic density protein PSD-95. Science *269*, 1737-1740.

Mottola, A., Antoniotti, S., Lovisolo, D., and Munaron, L. (2005). Regulation of noncapacitative calcium entry by arachidonic acid and nitric oxide in endothelial cells. Faseb J *19*, 2075-2077.

Philippides, A., Ott, S. R., Husbands, P., Lovick, T. A., and O'Shea, M. (2005). Modeling cooperative volume signaling in a plexus of nitric-oxide-synthase-expressing neurons. J Neurosci *25*, 6520-6532.

Rothman, J. S., and Manis, P. B. (2003). Kinetic analyses of three distinct potassium conductances in ventral cochlear nucleus neurons. J Neurophysiol *89*, 3083-3096.
Song, P., Yang, Y., Barnes-Davies, M., Bhattacharjee, A., Hamann, M., Forsythe, I. D., Oliver, D. L., and Kaczmarek, L. K. (2005). Acoustic environment determines phosphorylation state of the Kv3.1 potassium channel in auditory neurons. Nat Neurosci *8*, 1335-1342.
Wong, A. Y., Graham, B. P., Billups, B., and Forsythe, I. D. (2003). Distinguishing between presynaptic and postsynaptic mechanisms of short-term depression during action potential trains. J Neurosci *23*, 4868-4877.

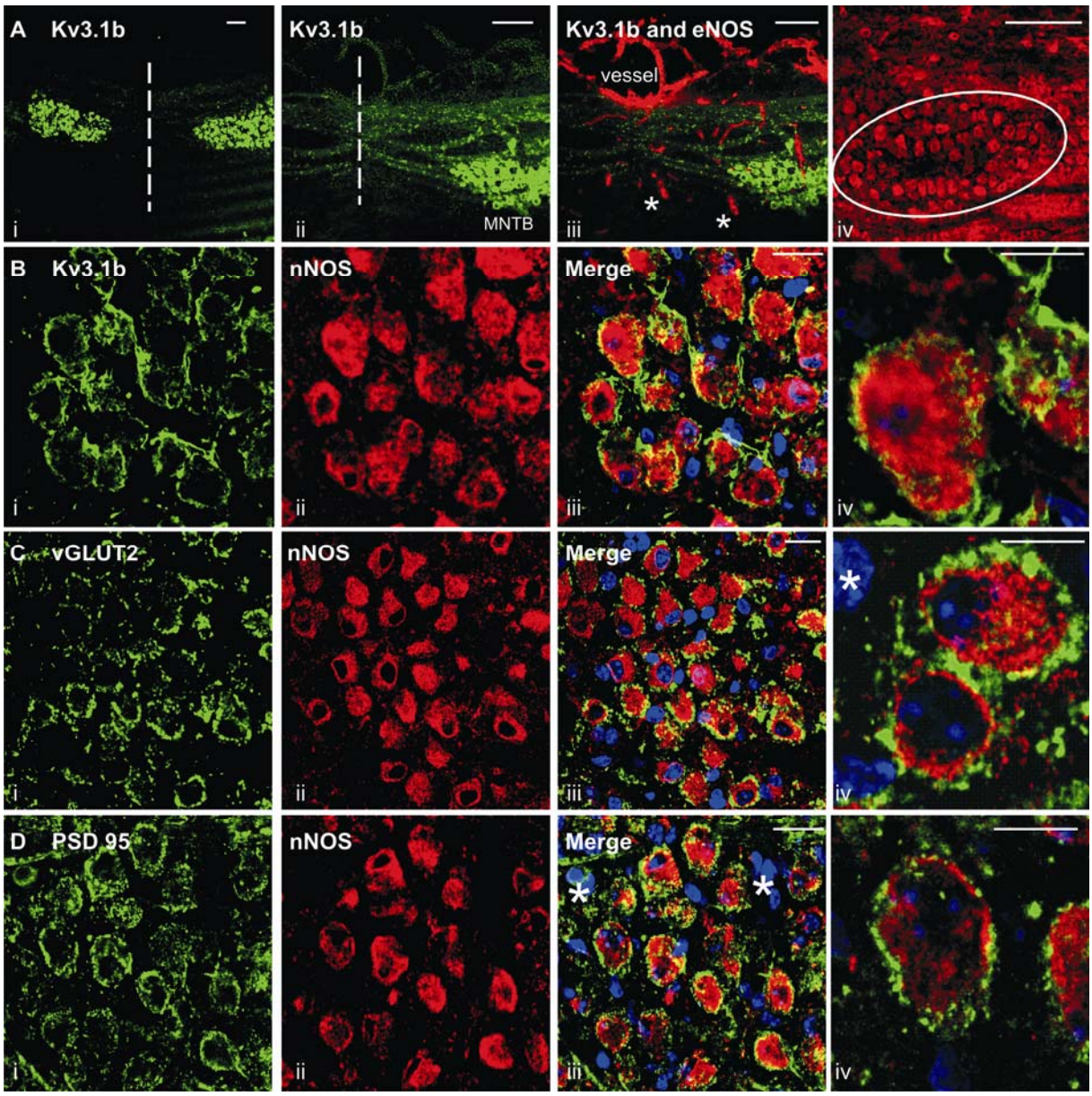
A Kv3.1b
Kv3.1b
MNTB
Kv3.1b and eNOS
vessel
B Kv3.1b
nNOS
Merge
C vGLUT2
nNOS
Merge
D PSD 95
nNOS
Merge

Fig1

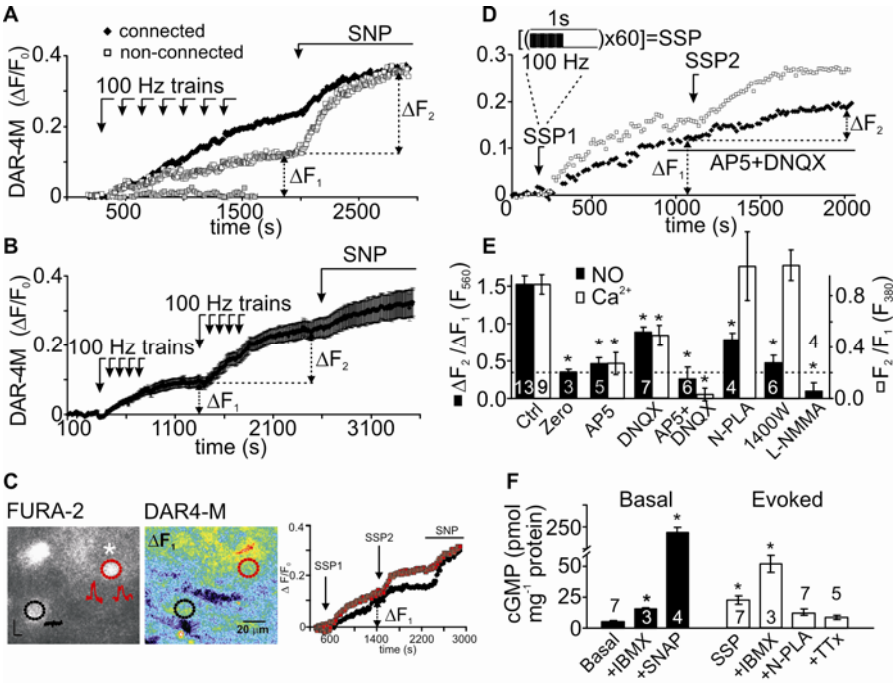
A
connected
non-connected
SNP
100 Hz trains
DAR-4M (ΔF/F0)
ΔF2
ΔF1
time (s)
B
SNP
100 Hz trains
100 Hz trains
DAR-4M (ΔF/F0)
ΔF2
ΔF1
time (s)
C
FURA-2
DAR4-M
ΔF1
SSP1
SSP2
SNP
ΔF1
20 μm
time (s)
D
1s
[( )x60]=SSP
100 Hz
SSP2
SSP1
ΔF2
ΔF1
AP5+DNQX
time (s)
E
NO
Ca2+
ΔF2 /ΔF1 (F560)
F2 /F1 (F380)
Ctrl
Zero
AP5
DNQX
AP5+ DNQX
N-PLA
1400W
L-NMMA
F
Basal
Evoked
cGMP (pmol mg-1 protein)
Basal
+IBMX
+SNAP
SSP
+IBMX
+N-PLA
+TTx

Fig 2

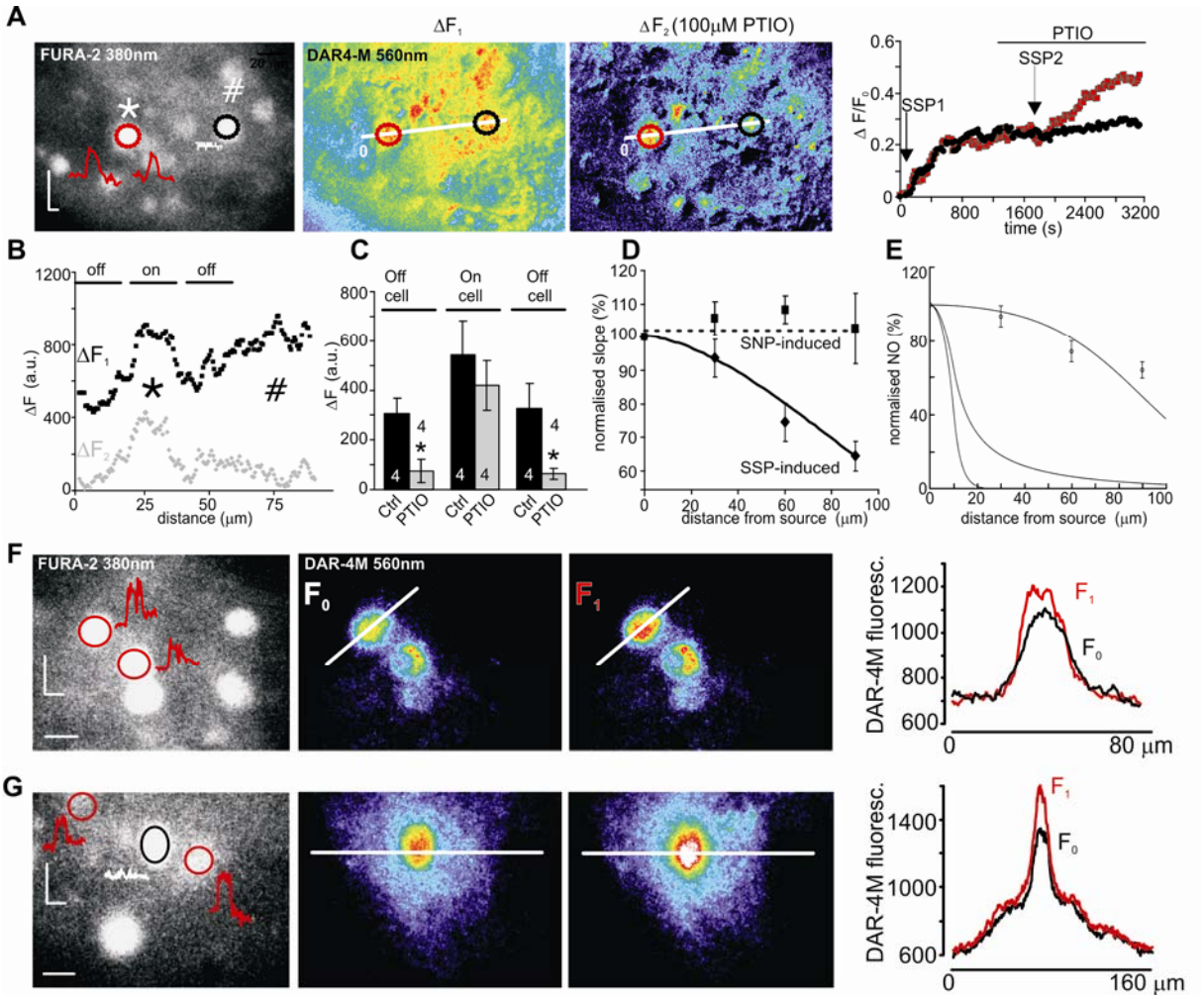
A
FURA-2 380nm
DAR4-M 560nm
ΔF1
ΔF2 (100μM PTIO)
PTIO
SSP1
SSP2
ΔF/F0
time (s)
B
off
on
off
ΔF1
ΔF2
ΔF (a.u.)
distance (μm)
C
Off cell
On cell
Off cell
Ctrl
PTIO
D
SNP-induced
SSP-induced
normalised slope (%)
distance from source (μm)
E
normalised NO (%)
distance from source (μm)
F
FURA-2 380nm
DAR-4M 560nm
F0
F1
DAR-4M fluoresc.
80 μm
G
160 μm

Fig 3

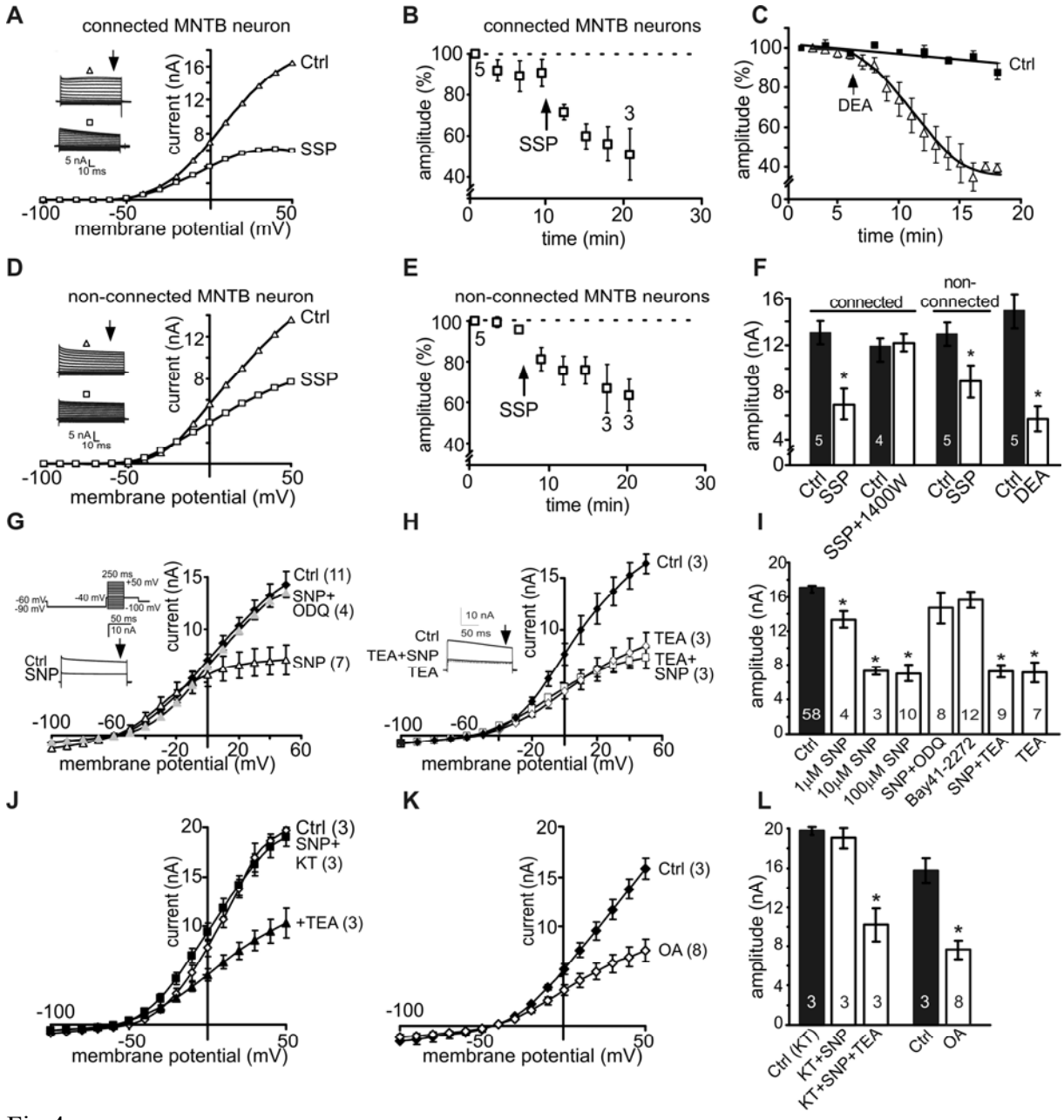
A
connected MNTB neuron
Ctrl
SSP
current (nA)
membrane potential (mV)
B
connected MNTB neurons
amplitude (%)
SSP
time (min)
C
Ctrl
DEA
amplitude (%)
time (min)
D
non-connected MNTB neuron
Ctrl
SSP
current (nA)
membrane potential (mV)
E
non-connected MNTB neurons
amplitude (%)
SSP
time (min)
F
connected
non-connected
amplitude (nA)
Ctrl
SSP
Ctrl
SSP+1400W
Ctrl
SSP
Ctrl
DEA
G
Ctrl (11)
SNP+
ODQ (4)
SNP (7)
Ctrl
SNP
current (nA)
membrane potential (mV)
H
Ctrl (3)
TEA (3)
TEA+
SNP (3)
Ctrl
TEA+SNP
TEA
current (nA)
membrane potential (mV)
I
amplitude (nA)
Ctrl
1μM SNP
10μM SNP
100μM SNP
SNP+ODQ
Bay41-2272
SNP+TEA
TEA
J
Ctrl (3)
SNP+
KT (3)
+TEA (3)
current (nA)
membrane potential (mV)
K
Ctrl (3)
OA (8)
current (nA)
membrane potential (mV)
L
amplitude (nA)
Ctrl (KT)
KT+SNP
KT+SNP+TEA
Ctrl
OA

Fig 4

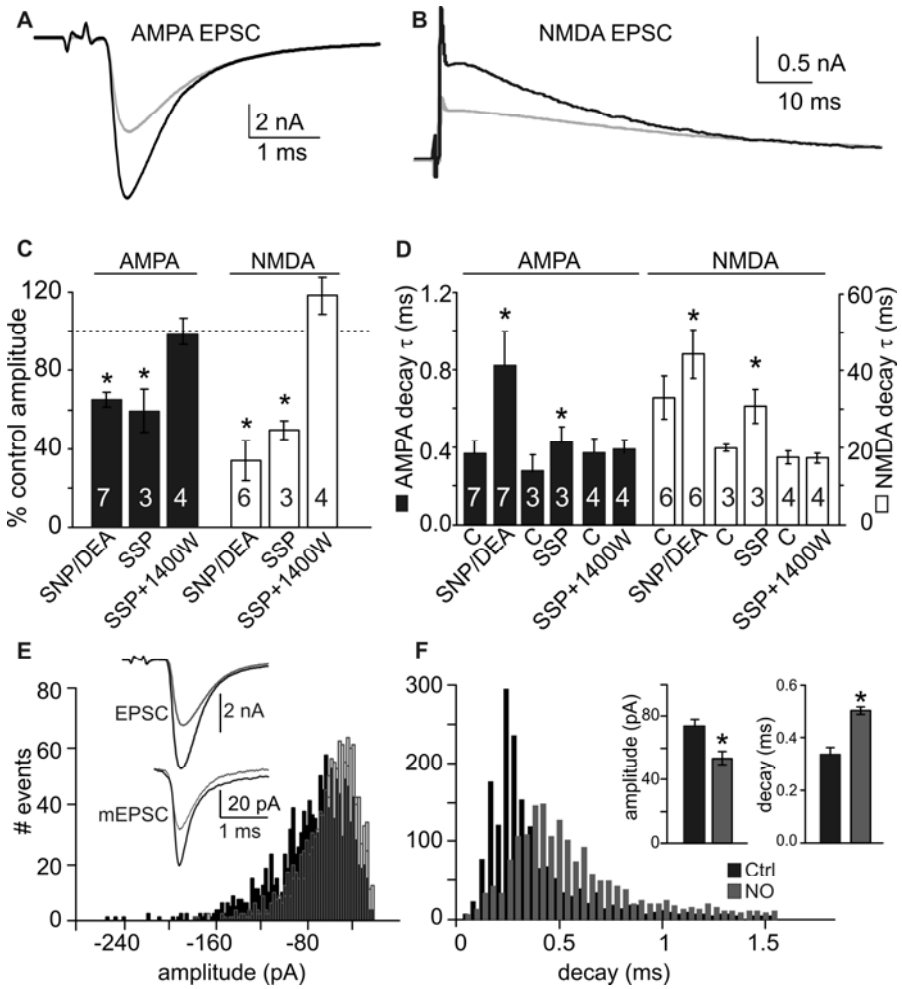
A
AMPA EPSC
2 nA
1 ms
B
NMDA EPSC
0.5 nA
10 ms
C
AMPA
NMDA
% control amplitude
120
80
40
0
7
3
4
6
3
4
SNP/DEA
SSP
SSP+1400W
SNP/DEA
SSP
SSP+1400W
D
AMPA
NMDA
AMPA decay τ (ms)
NMDA decay τ (ms)
1.2
0.8
0.4
0.0
60
40
20
0
7
7
3
3
4
4
6
6
3
3
4
4
C
SNP/DEA
C
SSP
C
SSP+1400W
C
SNP/DEA
C
SSP
C
SSP+1400W
E
events
80
60
40
20
0
EPSC
2 nA
mEPSC
20 pA
1 ms
-240
-160
-80
amplitude (pA)
F
300
200
100
0
0
0.5
1
1.5
decay (ms)
amplitude (pA)
80
40
0
decay (ms)
0.6
0.4
0.2
0.0
Ctrl
NO

Fig 5

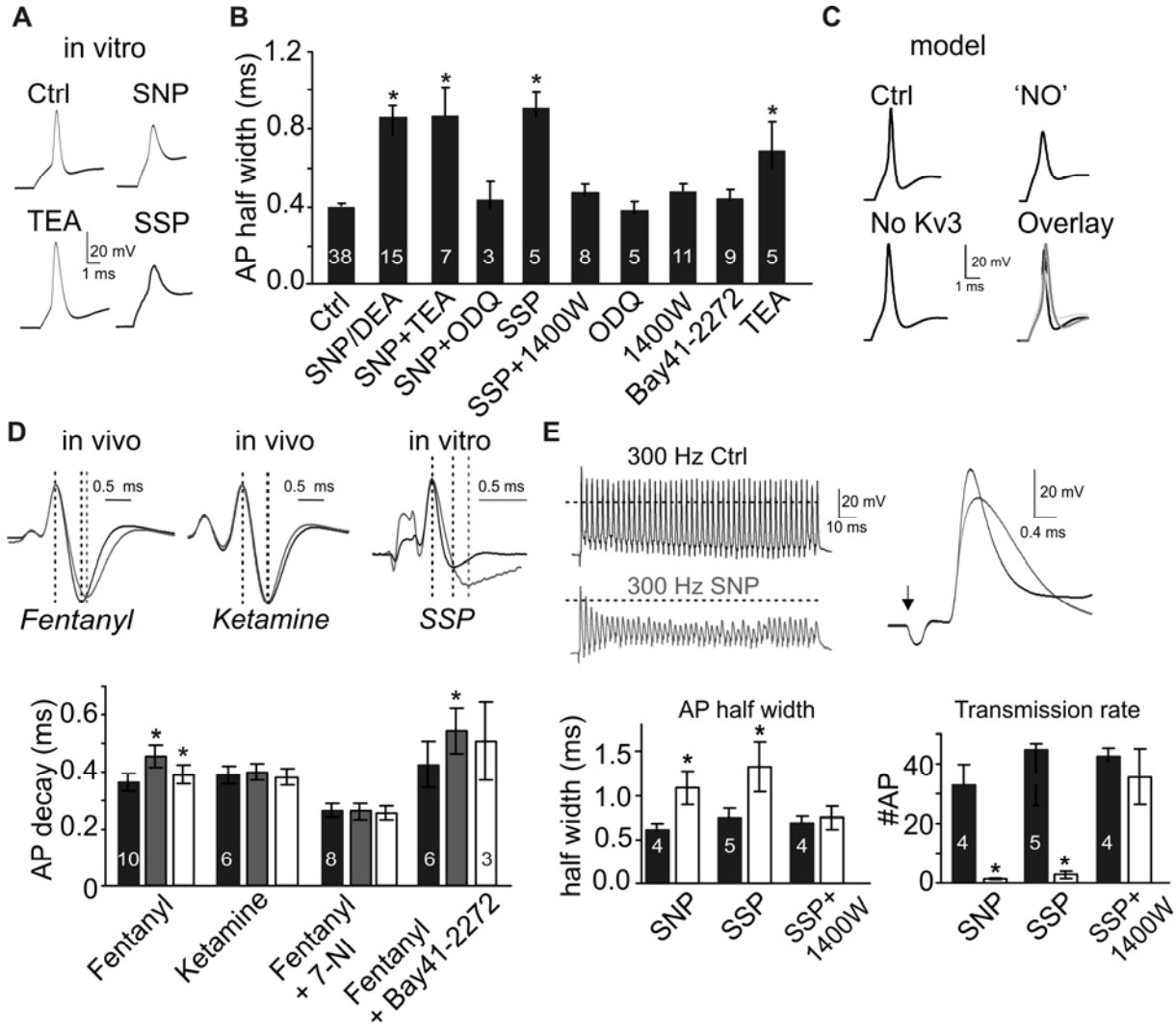
A
in vitro
Ctrl
SNP
TEA
SSP
20 mV
1 ms
B
AP half width (ms)
1.2
0.8
0.4
0.0
38
15
7
3
5
8
5
11
9
5
Ctrl
SNP/DEA
SNP+TEA
SNP+ODQ
SSP
SSP+1400W
ODQ
1400W
Bay41-2272
TEA
C
model
Ctrl
'NO'
No Kv3
Overlay
20 mV
1 ms
D
in vivo
in vivo
in vitro
0.5 ms
0.5 ms
0.5 ms
Fentanyl
Ketamine
SSP
AP decay (ms)
0.6
0.4
0.2
0
10
6
8
6
3
Fentanyl
Ketamine
Fentanyl + 7-NI
Fentanyl + Bay41-2272
E
300 Hz Ctrl
20 mV
10 ms
300 Hz SNP
20 mV
0.4 ms
AP half width
half width (ms)
1.5
1.0
0.5
0.0
4
5
4
SNP
SSP
SSP+ 1400W
Transmission rate
#AP
40
20
0
4
5
4
SNP
SSP
SSP+ 1400W

Fig 6

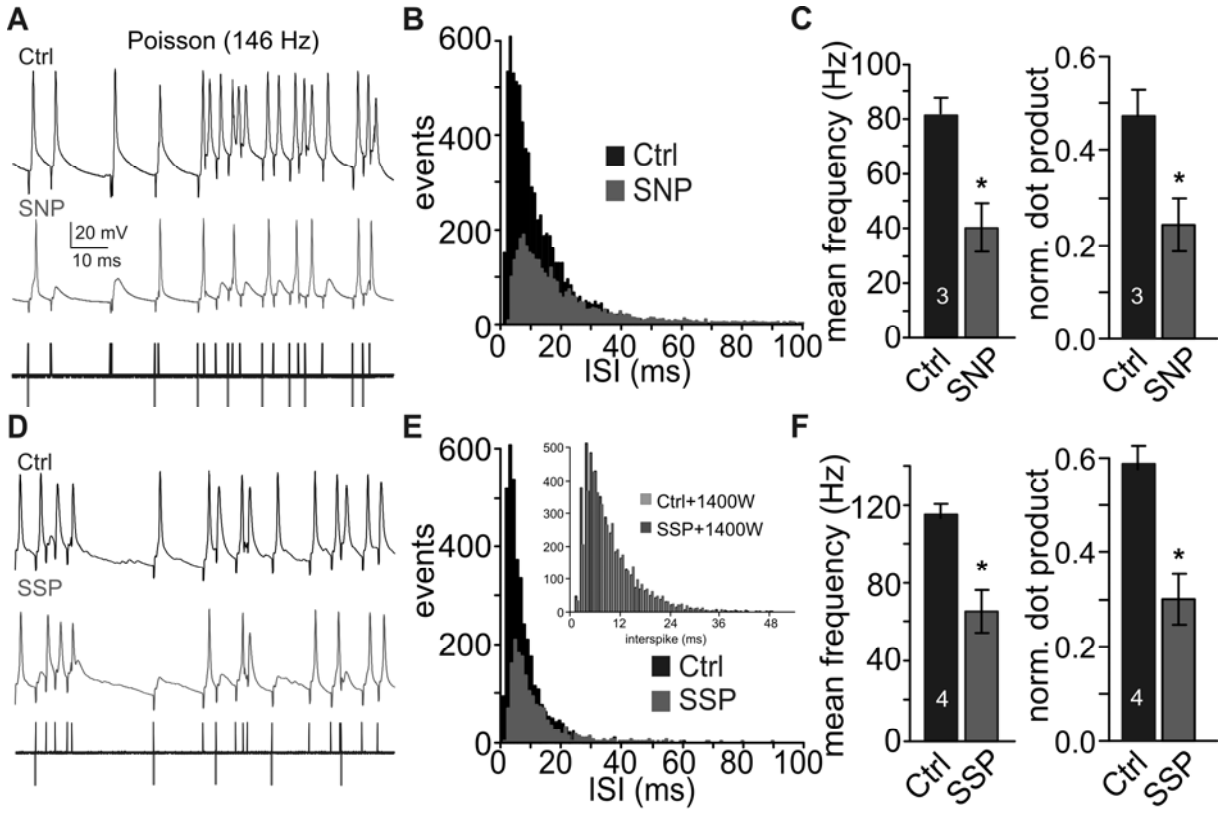
A
Poisson (146 Hz)
Ctrl
SNP
20 mV
10 ms
B
events
ISI (ms)
Ctrl
SNP
C
mean frequency (Hz)
norm. dot product
Ctrl
SNP
3
D
Ctrl
SSP
E
events
ISI (ms)
Ctrl+1400W
SSP+1400W
interspike (ms)
Ctrl
SSP
F
mean frequency (Hz)
norm. dot product
Ctrl
SSP
4

Fig 7

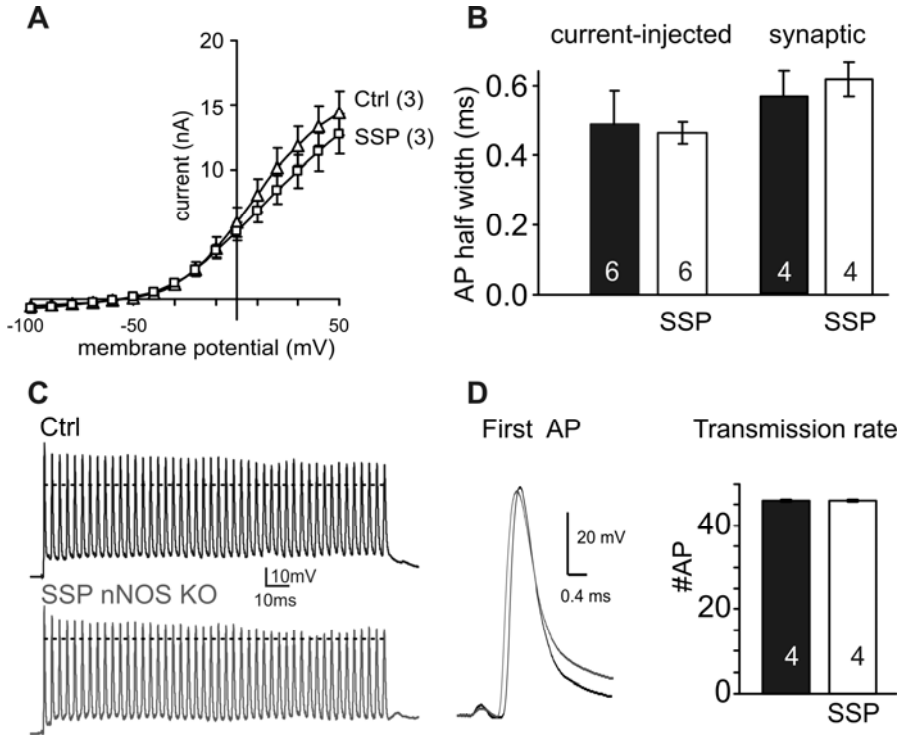
A
20
15
10
current (nA)
Ctrl (3)
SSP (3)
-100
-50
50
membrane potential (mV)
B
current-injected
synaptic
AP half width (ms)
0.6
0.4
0.2
0.0
6
6
4
4
SSP
SSP
C
Ctrl
10mV
10ms
SSP nNOS KO
D
First AP
20 mV
0.4 ms
Transmission rate
#AP
40
20
0
4
4
SSP

Fig 8

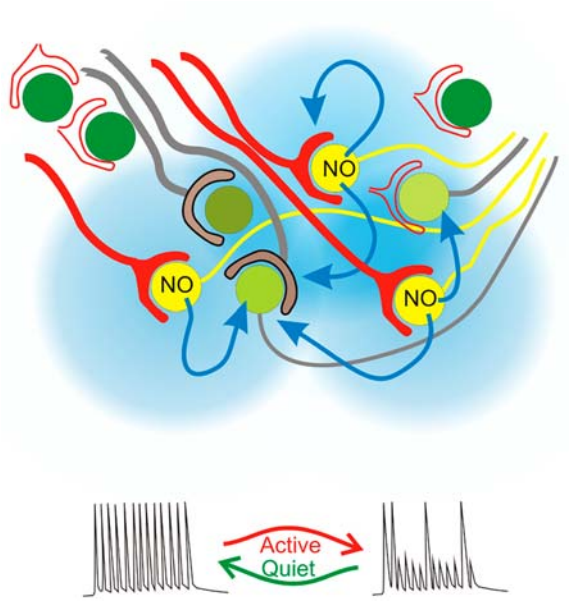

Fig 9